2018

Fabrication and Properties of Cu-SiC-GNP composites

Peijie Jia
University of Wollongong

UNIVERSITY
OF WOLLONGONG
AUSTRALIA

Fabrication and Properties of Cu-SiC-GNP composites

Peijie Jia

Supervisors:
Prof. Zhengyi Jiang and Dr. Haibo Xie

This thesis is presented as part of the requirement for the conferral of the degree:
Master of Research

University of Wollongong

School of Mechanical, Materials, Mechatronic and Biomedical Engineering

June 2018

Certification

I, Peijie Jia, declare that this thesis submitted in fulfillment of the requirements for the conferral of the degree Master of Research, from the University of Wollongong, is wholly my own work unless otherwise referenced or acknowledged. This document has not been submitted for qualifications at any other academic institution.

Peijie Jia

1st June 2018

Table of contents

Table of contentsList of figures I
List of figures IV
List of tables VII
List of abbreviation and symbol VIII
Abstract X
Acknowledgement XII
Chapter 1 Introduction 1
1.1 Background 1
1.2 Scope and objectives 2
1.3 Structure of chapters 2
Chapter 2 Literature review 4
2.1 Metal matrix composites (MMCs) 4
2.2 MMC reinforced with nanoparticles 5
2.3 Metal matrix composites reinforced with ceramic nanoparticles 7
2.4 Metal matrix composites reinforced with graphene sheets 12
2.5 Graphene/nanoparticles interaction: a road map to manufacture composites with exceptional properties 19
2.6 Manufacturing processes of metal matrix nanocomposites 21
2.6.1 Liquid processes 22
2.6.2 Solid processes 24
2.6.3 Semisolid processes 26
2.7 Strengthening mechanisms of MMnCs 29
2.7.1 Load transfer effect 29
2.7.2 Hall-Petch strengthening 30
2.7.3 Orowan strengthening 31
2.7.4 CTE and EM mismatch 31
2.7.5 Sum of contributions 32
2.8 Summary 33
Chapter 3 Experimental methodology 35
3.1 Sample preparation 35

3.1.1 Ball milling 35
3.1.2 Cold pressing and sintering 36
3.2 Experiment and analysis 38
3.2.1 Hot mounting, grinding and polishing 38
3.2.2 KEYENCE laser microscope (3D & profile measurement) and density measuring instrument 40
3.2.3 X-ray diffraction 41
3.2.4 Microhardness testing 42
3.2.5 Field emission scanning electron microscopy 43
3.2.6 Compression test 44
Chapter 4 Effect of sintering temperature 45
4.1 Introduction 45
4.2 Experimental procedure 45
4.3 Results and discussion 45
4.3.1 Pure copper 45
4.3.1.1 Optical images 45
4.3.1.2 Density measurement 47
4.3.1.3 Microhardness testing 48
4.3.2 Cu-SiC-GNP 49
4.3.2.1 Optical images 49
4.3.2.2 Density measurement 50
4.3.2.3 Microhardness testing 51
4.4 Summary 52
Chapter 5 Effect of milling time 53
5.1 Introduction 53
5.2 Experimental procedure 53
5.3 Results and discussion 53
5.3.1 Powder analysis 53
5.3.1.1 SEM 53
5.3.1.2 XRD analysis 57
5.3.2 Analysis of sintered composites 63
5.3.2.1 Optical images 63
5.3.2.2 Density measurement 67
5.3.2.3 Microhardness testing 70

5.3.2.4 Compressive testing 73
5.4 Summary 76
Chapter 6 Conclusion and future work 79
6.1 Conclusions 79
6.2 Future work 81
References 83

List of figures

Figure 2-1 Optical images of Cu-SiC composites. 9

Figure 2-2 Apparent density vs. milling time. 10

Figure 2-3 Volume loss vs. sliding distance. 11

Figure 2-4 Bright-field TEM image showing graphene agglomerations. 14

Figure 2-5 Fractures microphotography: (a) Cu-5% graphite, (b) Cu-5% CNFs and (c) Cu-3% graphene 15

Figure 2-6 Tensile stress-strain curves of Cu and GNS-Ni/Cu. 18

Figure 2-7 Schematic of Cu-graphene deposited on Cu substrate. 18

Figure 2-8 Processes of MMCs 21

Figure 2-9 Phase stability diagram for Si-C-O at 1680 K & the equilibrium constant vs. temperature (K). 23

Figure 2-10 Equipment of electroforming. 24

Figure 2-11 SEM images of fracture surfaces: (a) Al6061-1.0 wt.% with milling time of 90 min, and (b) unalloyed Al6061 with a milling time of 90 min. 27

Figure 2-12 The average thermal conductivity with volume fraction of of Al2O3. 27

Figure 2-13 Tensile strength at different temperature. 28

Figure 2-14 (a) Morphology of mixed powder, and (b) high magnification image of (a). 28

Figure 2-15 FE-SEM images of TiC/Ti nanocomposites 29

Figure 3-1 Fritsch pulverisette 6 planetary mono mill 35

Figure 3-2 Schematic of dies. 37

Figure 3-3 Heating curve of sintering. 38

Figure 3-4 (a) 10 Tonne hydraulic press and (b) KTL 1400 tube furnace. 38

Figure 3-5 Struers citopress 20 hot mounting. 39

Figure 3-6 Struers TegralPol-21 automatic grinding/polishing machine. 39

Figure 3-7 (a) KEYENCE laser microscope and (b) automatic density measuring instrument. 40

Figure 3-8 GBC MMA XRD. 41

Figure 3-9 Schematic of the indenter and indentation of vickers hardness. 42

Figure 3-10 TIME TH7 15 microhardness tester. 43

Figure 3-11 JEOL JSM-7500FA field emission scanning electron microscope (FESEM) 44

Figure 3-12 500 KN Instron universal testing machine. 44

Figure 4-1 Optical micrographs of pure copper samples sintered at (a) 700 ºC, (b) 750 ºC, (c) 800 ºC, (d) 850 ºC and (e) 900 ºC. 46

Figure 4-2 Density of as-received copper powder compacted in 850 MPa vs. sintering temperature. 47

Figure 4-3 Vickers micro-hardness of as-received copper powder compacted in 850 MPa vs. sintering temperature. 48

Figure 4-4 Optical micrographs of Cu-SiC-GNP composite (milled for 2 h) sintered at (a) 700 ºC, (b) 750 ºC, (c) 800 ºC, (d) 850 ºC and (e) 900 ºC. 50

Figure 4-5 Density Cu-SiC-GNP (milled for 2 h and compacted in 850 MPa) vs. sintering temperature. 51

Figure 4-6 Vickers microhardness of Cu-SiC-GNP composite (milled for 2 h and compacted for 850 MPa) vs. sintering temperature. 52

Figure 5-1 SEM micrographs of (a) as-received pure Cu powders and (b) 2 h, (c) 4 h, (d) 6 h and (e) 8 h pure Cu powders milled. 54

Figure 5-2 SEM micrographs of and (a) 2 h, (b) 4 h, (c) 6 h, (d) 8 h and (e) 20 h Cu-SiC powders milled. 56

Figure 5-3 SEM micrographs of (a) 2 h, (b) 4 h, (c) 6 h and (d) 8 h Cu-SiC-GNP powders milled. 57

Figure 5-4 XRD patterns of Cu milled for 0, 2, 4, 6 and 8 h. 58

Figure 5-5 W-H plots for Cu powder milled for 2 h. 58

Figure 5-6 Grain size vs. milling time for copper powder. 59

Figure 5-7 XRD patterns of the as-received pure copper powder and Cu-SiC powder milled for 2, 4, 6, 8, 12, 16 and 20 h. 60

Figure 5-8 Grain size vs. milling time for Cu-SiC powder. 61

Figure 5-9 XRD patterns of the as-received pure copper powder and Cu-SiC-GNP milled for 2, 4, 6 and 8 h. 62

Figure 5-10 Grain size vs. milling time for Cu-SiC-GNP powder. 63

Figure 5-11 Optical micrographs of Cu milled for (a) 2 h, (b) 4 h, (c) 6 h and (d) 8 h. 64

Figure 5-12 Optical micrographs of Cu-SiC milled for (a) 2 h, (b) 4 h, (c) 6 h and (d) 8 h. 65

Figure 5-13 Optical micrographs of Cu-SiC-GNP milled for (a) 2 h, (b) 4 h, (c) 6 h and (d) 8 h. 66

Figure 5-14 Density of milled copper vs. milling time of 2, 4, 6 and 8 h. 68

Figure 5-15 Density Cu-SiC composite vs. milling time of 2, 4, 6 and 8 h. 69

Figure 5-16 Density of Cu-SiC-GNP vs. milling time of 2, 4, 6 and 8 h. 70

Figure 5-17 Hardness of copper vs. milling time of 2, 4, 6 and 8 h. 71
Figure 5-18 Hardness of Cu-SiC vs. milling time of 2, 4, 6 and 8 h. 72
Figure 5-19 Hardness of Cu-SiC-GNP vs. milling time of 2, 4, 6 and 8 h. 73
Figure 5-20 Compressive strain-stress curves of Cu milled for 0, 2, 4, 6 and 8 h..... 74
Figure 5-21 Compressive strain-stress curves of Cu-SiC milled for 2, 4, 6 and 8 h. .. 75
Figure 5-22 Compressive strain-stress curves of Cu-SiC-GNP milled for 2, 4, 6 and 8 h..... 76

List of tables

Table 2-1 Fabrication methods for MMnCs.....26
Table 3-1 Chemical composites of as-received copper powder.....36
Table 3-2 Parameters of ball milling.....36
Table 4-1 Density of samples made of the as-received copper powder.....47
Table 4-2 Hardness of samples made of the as-received copper powder. 48
Table 4-3 Density of samples made of the Cu-SiC-GNP powder.....50
Table 4-4 Hardness of samples made of the Cu-SiC-GNP powder. 51
Table 5-1 Density of samples made of the milled copper powder.....67
Table 5-2 Density of samples made of the Cu-SiC powder. 68
Table 5-3 Density of samples made of the Cu-SiC-GNP powder.....69
Table 5-4 Results of compression testing of Cu. 74
Table 5-5 Results of compression testing of Cu-SiC. 75
Table 5-6 Results of compression testing of Cu-SiC-GNP. 76

List of abbreviation and symbol

1. Abbreviation

AR	as-received
BPR	ball to powder weight ratio
CMC	ceramic matrix composites
CNF	carbon nanofibers
CTE	coefficient of thermal expansion
CVD	chemical vapor deposition
DC	direct current
EDS	energy-disperse X-ray spectroscopy
EM	elastic modulus
FESEM	field emission scanning electron microscopy
FSP	friction stir processing
GNDs	geometrically necessary dislocations
GNF	graphene nanoflakes
GNP	graphene nanoplate
GNSs	graphene nanosheets
GO	graphene oxide
Gr	graphite
HIP	hot isostatic pressing
L/D	length-to-diameter ratio
MA	mechanical alloying
MLG	multi-layer graphene
MM	mechanical milling
MMC	metal matrix composites
OM	optical microscopy
PC	pulse current
PCA	process control agent

PM	powder metallurgy
PTFE	Polytetrafluoroethylene
rGO	reduced graphene oxide
RPM	revolutions per minute
SEM	scanning electron microscopy
TEM	transmission electron microscope
UTS	ultimate tensile strength
W-H	William-Hall
XPS	X-ray photoelectron spectroscopy
XRD	X-ray diffraction
YS	yield strength

2. Symbol

A	amp
Å	angstrom
ºC	Celsius degree
h	hour
HV	unit of vickers hardness
min	minute
MPa	Mega Pascal
°	degree
s	second
µm	micrometer
v	volt
vol%	volume percent
wt%	weight percent

Abstract

Based on the unique structure and excellent properties of graphene, the graphene nanoplates (GNP) were added to the traditional Cu-SiC composites. In this study, planetary ball milling, cold pressing and sintering were utilised to fabricate the Cu-SiC-GNP composites, which might be a route of the efficient industrial manufacturing of Cu-SiC-GNP composites.

As for a new material, processing parameters of Cu-SiC-GNP needed to be investigated first. At the beginning of study, the as-received copper and Cu-SiC-GNP milled for 2 h were used to find an appropriate sintering temperature. Morphology, density and hardness were all employed and analysed. The connection of grains for Cu and Cu-SiC-GNP tended to increase while the ratio of pore and void inclined to decrease. Considering both curves of density vs. sintering temperature and curves of microhardness vs. sintering temperature, the best sintering temperature for these two kinds of materials was 800 °C. Furthermore, it was found that sintering of Cu-SiC-GNP composites was harder because of the addition of SiC and GNP with higher melting points.

In the analysis of ball milling time, pure Cu and Cu-SiC were used as a comparison to Cu-SiC-GNP. Both the powders and bulk samples were analysed through the XRD, FSEM, optical microscope, automatic density measuring machine, Vickers microhardness testing machine and universal testing machine. The X-ray diffraction (XRD) result showed that there was no undesirable or just a slight volume of unexpected reaction happened within 8 h ball milling. The morphology of Cu, Cu-SiC and Cu-SiC-GNP showed the similar trend after 8 h ball milling in which most laminar (flake) particles were formed, attributing the cold welding and fracturing. In addition, densities of these three materials declined with the increase of ball milling time due to the work hardening and irregular shapes of particles. In term of hardness, the hardness

of all the three materials inclined to increase generally with the increase of ball milling time, attributed to the work hardening and the refinement of particles. Whereas there was enhancement in compressive properties of Cu and Cu-SiC, the maximum of compressive stress of Cu-SiC-GNP had a tendency to decrease with the prolonged ball milling time. In addition, the yield point of Cu-SiC-GNP changed irregularly with the increase of ball milling time, which could be attributed to irregular morphology of Cu-SiC-GNP particles and the ball milling time that was not long enough to disperse both the SiC nanoparticles and graphene nanoplates homogeneously in the Cu matrix.

In ball milling of Cu-SiC-GNP, the deformation and work hardening could be the main mechanism that strengthened the hardness and decreased the density with the increase of ball milling time. Furthermore, locally high internal strain was caused by the resistance to further deformation that brought about the increase of dislocation densities and grain refinement, and it increased the hardnesss. The strengthening mechanism for the compressive strength for Cu-SiC-GNP could be ascribed to: (i) grain refinement, (ii) load transferring from the matrix to the SiC nanoparticles and GNP, and (iii) increase in dislocation caused by the mismatch between the matrix and reinforcements.

This study is a fundamental investigation of Cu-SiC-GNP composites to find out the appropriate processing parameters, the evolution of powders during milling and basic mechanical properties of the new material. In near future, a longer ball milling time of Cu-SiC-GNP will be studied to observe the variations of the powder material and bulk material. Additionally, other identification methods like etching will be used to obtain a clear distribution of porosity. Furthermore, tensile test and tribological measurement will be conducted to reveal the wear resistance of Cu-SiC-GNP composites.

Keywords: sintering temperature, ball milling time, morphology, density, hardness, compressive property.

Acknowledgement

I want to express my sincere appreciation to my supervisor Prof. Zhengyi Jiang who gives me such a big opportunity to study at University of Wollongong (UOW) as a Master of Research student. Since I came here, Prof. Jiang has affected me with his endeavour and enthusiasm in research, as a role model in my way to scholarship. Moreover, he has been giving me encouragement and confidence in the semester. I am very grateful for his help in choosing my research and solving my problems in writing my thesis. Additionally, I benefit a lot from the discussion about my research with him.

I am very grateful for Prof. Huiqin Chen who gives me a good advice to come to UOW for further study. During my time in Taiyuan University of Science and Technology (TYUST), Prof. Chen is very strict with my study, which is quite helpful for my study in UOW. The related learning in TYUST prepares me with a good technical knowledge base and the right attitude to research.

My sincere acknowledgement also goes to my co-supervisor Haibo Xie, a heart-warming and mild Chinese man. He does a great job in assist HDR students in writing their thesis and preparing for presentation. He always greets me with a big smile, just like a close family.

It is unforgettable for me that Mathew Franklin gives me the first induction in his lab. He does very well in the introduction of the polishing machines, the mounting machine and so on. Furthermore, Wayne Ireland for his commitment to the safety check. It is nice of Vick Mackie for the training of XRD, Vitor Sencadas for the instruction of the hydraulic pressing machine, and Duncan Best for the universal testing machine as well.

It could not be forgotten that my teammate Jiangshan Zhang helped in walk through the route to my research. His attitude and scholar into his research really teach me to be

earnest and keep in progress with the new papers about my research. I am grateful for the help and assistance from Fanghui Jia and Wenzheng Xia as well.

Last but not the least, I thank my whole family for funding me to complete my study in UOW. Thank UOW in Australia for providing me with a chance to study here and enjoy the wonderful journey in my life.

Chapter 1 Introduction

1.1 Background

It has been widely studied in Cu-SiC composites for their excellent thermal and electrical conductivities, superior wear resistance, frictional properties and hardness. These composited have been applied to the electrical contacts and welding electrodes [1-4]. For the composite materials reinforced with particles, it is required to distribute homogeneously for the reinforcing phases in the matrix to bring a superior performance [5].

Particle agglomeration could be brought for differences in geometries, densities, flow of electrical charges, especially in the nanoparticles [6]. Lots of manufacturing routes have been employed to solve the problem through powder metallurgy, stir casting, flake powder metallurgy, semi-solid powder processing and ultrasonic-assisted casting [7-15]. In the powder metallurgy route, the mixing of the matrix and reinforcement is crucial for reinforcement to distribute in the matrix homogeneously [16, 17]. Among all the methods, mechanical milling is one that is capable to enhance the particle distribution, which incorporates the reinforcement particles into the matrix within a close range [18-20]. It is found that the repeated fracturing and cold welding of particles is the major mechanism during the structuring microstructures, attributed to the collisions between the powders and the milling balls [21]. However, disadvantages are brought like the decrease in the compressibility of powders caused by the cold worked structure and the contamination of powders due to the gas during sintering [22-24].

In addition, single reinforcements like SiC might bring about deterioration in physical properties. Moreover, there are just a few of reports about adding new material to improve the properties of traditional Cu-SiC composites. Hence, this study conducts a research that adds graphene nanoplates (GNP) into the traditional SiC nanoparticles

reinforced Cu matrix composites, changing the microstructure of composites and conferring improvements in the mechanical properties compared to the traditional Cu-SiC composites. The material has never been studied before. Therefore, this research focuses on finding out the appropriate experimental parameters such as sintering temperatures and ball milling time for the new material. At the same time, morphology, XRD patterns of powders will be investigated and analysed. Furthermore, morphology, density, hardness and compressive properties of sintered samples will be studied.

1.2 Scope and objectives

The objective of this study is mainly to investigate the effects of added GNP on the microstructure and mechanical properties of copper matrix composites reinforced with SiC nanoparticles. The aim is to study effects of sintering temperatures and ball milling time on the morphology and fundamental properties of samples after GNP is added.

In this study, the crystallite size is calculated by the William-Hall (W-H) method based on the XRD patterns, and chemical components are analysed through XRD patterns as well. Additionally, the morphology and properties of powder samples are investigated by the FSEM. Strengthening mechanisms are discussed to explain the nanostructural evolutions and the shift in relevant properties as well.

Pure copper and Cu-SiC composites are fabricated as a comparison to the Cu -SiC-GNP nanoparticles.

1.3 Structure of chapters

This chapter represents the background of Cu matrix composites in this study. In addition, the aims and scope of the research are given in the chapter as well. The structure of all the chapters is discussed below.

Chapter 2 is about the literature review introducing the metal matrix composites, then the copper matrix composites reinforced with nanoparticles. In addition, graphene reinforced ceramic composites and copper matrix composites are introduced and concluded as well. Furthermore, the processing routes and strengthening mechanism of MMnCs are presented. At the same time, relevant researches are put forward.

Chapter 3 includes the processing of fabrication and the relevant devices applied to this study, involving the materials information, the parameters and basic principles of this study and devices.

Chapter 4 is about the fabrication and results of pure copper samples and Cu-SiC-GNP milled for 2 h, which is to investigate an appropriate sintering temperature. Density, hardness and morphology are measured to analyse the variation with the increase of sintering temperatures.

Chapter 5 shows the fabrication and results of Cu, Cu-SiC composites and Cu-SiC-GNP composites milled for different time. Both the powders and bulk samples are analysed through the XRD, FSEM, optical microscope, automatic density measuring machine, Vickers microhardness testing machine and universal testing machine.

Chapter 6 summarises the current results obtained in this study. Additionally, more studies and experiments are put forward as well to investigate physical and mechanical properties of the Cu matrix composites achieved in this study. Moreover, more processing parameters like different ratio of SiC and GNP should be investigated to obtain different composites, which could be utilised to fabricate various components such as welding electrodes and electrical contacts.

Chapter 2 Literature review

2.1 Metal matrix composites (MMCs)

The definition for MMCs is not simple or clear for the complexity of its components. MMCs first appeared in the military systems as a unique technology. It has been applied widely to structural enforcement, thermal management, precision devices, wear resistance and so on. By far most commercial composites matrices are Al, Cu, Mg, Ni, Ag, Be, Fe, Ti and Co [25].

Production methods have been developed into like casting, wet chemistry and powder metallurgy methods. There have been new reinforcements such as platelets and fibers [26]. Furthermore, new metal composites emerge such as hybrid material using the kerf loss waste and flush waste [27]. The research showed the increase of reinforcing particles are applied, which contain metal borides (TaB_2, TiB_2, WB, ZrB_2) and metal carbides (SiC, TaC, B_4C, WC), metal oxides and metal nitrides [26].

Dated back to the late 1960s, MMCs were applicated for the first time because of the exploitation of a steel-wire reinforced copper alloy [28]. Now, copper matrix composites are widely employed in production as electrical-contact materials in contactors, switches, because there are lots of excellent mechanical and physical properties about copper, like high electrical and thermal conductivity, excellent corrosion and wear resistance high tensile strength and Young's modulus as well as lower coefficient of thermal expansion (CTE) than that of aluminum [29, 30].

As a result, they are thought to be utilised in the scope like heat sinks, electronic packages and fuel cell electrodes. However, drawbacks like high density and low hardness are so obvious that they must be overcame through adding reinforced phases [31, 32].

Currently, copper matrix composites have three main forms: microscope copper alloy, particle reinforced copper matrix composites and fiber reinforced copper matrix composites. Primary processing methods includes powder metallurgy, cold pressing then by forging or extrusion and heat treatment if necessary [26].

There are different kinds of reinforcing ceramic particles employed in copper matrix composites in which SiC and Al_2O_3 are most common [33, 34]. It is found that SiC reinforced copper matrix composite contact material there is no other phase apart from Cu and SiC, which is through sintering process. Although the hardness of composite is raised because of dispersion of SiC particles improving the strength by impeding the dislocation, but weight loss and oxidation occur during the contact-count experiments [29].

2.2 MMC reinforced with nanoparticles

Conventional ceramic-reinforcing MMCs show high elastic modulus and strength, near- isotropic and high-temperature creep resistant properties, but the particulates sizes are large, ranging from a few to several hundred micrometers. During mechanical loading, the large-size particles are prone to cracking, producing low ductility and premature failure of composites [35].

In 2004, nanotechnology was explained as “The creation, processing, and characterization of materials, devices, and systems with dimension on the order of 0.1-100 nm, exhibiting novel and significantly enhanced physical, chemical, and biological properties, functions, phenomena, and processes due to their nanoscale size”. Different component materials will cause their difference in mechanical, thermal, electrochemical, catalytic, electrical and optical properties. Furthermore, certain size of particles govern properties of materials [36].

Nanoparticles reinforced MMCs can be regarded as promising alternative, which could overcome the restriction of MMCs reinforced with micron-sized particles [37]. However, there is a challenge in the manufacturing metal matrix composites reinforced with nanoparticles, on account of difficulty in achieving a uniform distribution for the nanoparticles within metal matrix [35]. Most used nanoparticles are SiC, TiC, TaC, Al_2O_3, and AlN. Additionally, the most common techniques employed in processing metal matrix nanocomposites are rapid solidification, vapor techniques, liquid metal infiltration, electrodeposition and chemical methods.

Apart from nanoparticles, discontinuous nanofiller like nano-fibers, nano-wires and nanoplatelets have been taken as reinforcements alternative, which is a development trend [36].

The fracture mode is inter-granular fracture with respect to monolithic metal, while it changes to trans-granular fracture mode for nanocomposites, causing enhanced tensile properties, super high-temperature stability of structure, increased fracture toughness, enhanced creep, wear resistance and thermal shock.

It is approved that mechanical, thermal, catalytic, electrical and electrochemical properties of nanocomposites could be significantly enhanced below a threshold size. It is still a debate among researches about strenghthening mechanism by which nanoparticles augment properties of composites [36].

Compared to the production by using micron-sized particles, it has shown that the way nanoparticles incorporated within the metallic matrices could cause the increase in mechanical properties, which is strengthened because of dispersion of particles under different load content. For example, it has been found that the yield strength and elastic modulus can be augmented through decreasing the reinforcement size to the nanometric

scale [38].

The nature of boding between the matrix and nano-reinforcement could be the principal factor affecting mechanical properties of composites. Furthermore, it has been widely acknowledged that reducing the size of reinforcement and grains could enhance mechanical properties like hardness and strength, attributed to the increased effective barriers that inhibit the dislocation moving through the matrix [39]. Nonetheless, there are drawbacks in the strategy, which decreases the ductility and increases high creep rate along with reducing the grain size. It is approved that mechanical properties of nanocrystalline materials are not extremely authentic, ascribed to the augment of the porosity content of materials owing to insertion of microvoids related to the incorporation of nanoparticles within the matrix [40]

It is demonstrated by a lot of studies that uniform distribution of nanoparticles, volume fraction of nanoparticles within the matrix and properties of nano-level powders are significantly associated with mechanical characteristics of nanocomposites [41].

Nevertheless, it is such a challenge for nanoparticles to distribute uniformly within metallic matrices in liquid and solid processing routes, attributed to the high propensity of agglomeration of particles and other interactive phenomena like electro-repulsion, especially at huge volume fractions, which diminishes mechanical properties including the elastic modulus and fracture toughness [38, 42].

2.3 Metal matrix composites reinforced with ceramic nanoparticles

Copper offers a lot of excellent properties like good formability, thermal conductivity, excellent electrical conductivity and low cost, which makes copper an appropriate candidate to fabricate copper matrix composites for functional and structural applications [43, 44]. However, poor properties like low hardness, tensile and creep

strength make it restricted at ambient and high temperatures [45].

It is documented that reinforcement particulates reinforced copper matrix composites can be significantly improved in the wear resistance and high-temperature mechanical properties without severe deterioration of electrical and thermal conductivities of the copper [46].

The common reinforcement particles such as alumina, silicon carbide, titanium carbide or a combination of these materials have presented more superior advantages than copper alloys [47].

Al_2O_3, SiO_2, SiC and MgO nanoparticles reinforced copper matrix composites are fabricated by powder metallurgy [48]. It is found that the coefficient of thermal expansion (CTE) is reduced through introducing dispersed nanoparticles in the copper matrix. By contrast, CTE and the interfacial pressure could be raised by increase of the temperature, and calculated pressure values are consistent with variations observed.

Shehata et al. [49] utilised two different routes to synthesise the Cu-Al_2O_3 nano-sized powders, which add Cu to aqueous solution of aluminum and solution of ammonium hydroxide and aluminum nitrate separately, and it is found that finer alumina particles were achieved by the second route, meanwhile, copper aluminate structure formed at copper-alumina interface.

Among particles reinforced copper matrix composites, SiC particles (SiCp) reinforced copper matrix composites receive wide attention, due to high thermal conductivity, high melting point, good mechanical properties like high anti-wear stiffness, high hardness and low costs of production [50]. These composites could be employed widely as electrical contact materials such as contactors, circuit breaks, electronic packaging and relays that require fine electrical and thermal conductivity as well as brazing and

welding properties [51].

Efe et al. [52] investigated the sintering temperatures of Cu-SiC composites fabricated by PM. As displayed in Figure 2-1, it was found that reinforced SiC particles obtained a uniform distribution in the matrix. Furthermore, the hardness and electrical conductivity increased with the increase of sintering temperature, attributing to a more homogeneous microstructure at 900 ºC. The optimal sintering temperature was 900 ºC. Nevertheless, the density decreased when the temperature rose to 900 ºC. At the same time, a peak of Cu_2O was found in the XRD pattern, which meant oxidation might happen during sintering under the open atmosphere.

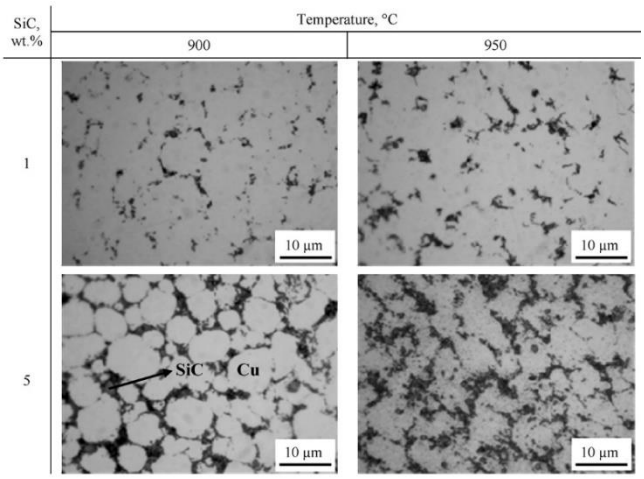

Figure 2-1 Optical images of Cu-SiC composites.

Rahimian et al. [53] investigated the sintering temperature of Al-Al_2O_3 made by powder metallurgy (PM) as well. It was mentioned that porosity variations with the size of alumina particles, ascribed to a better compressibility of bigger particles. For instance, it was pointed that porosity could be decreased with the elevated sintering temperatures [54]. Additionally, it was found that prolonged sintering time might cause the hardness to decline. In addition, higher elongations were achieved with extended sintering times and finer alumina.

Cabeza et al. [55] synthesised the AA 6005A reinforced with TiC particles by ball

milling. It was found that finer size of matrix particles and homogeneous distribution of TiC particles could be attained by increasing the ratio of reinforcement particles. No contamination was identified after ball milling. Furthermore, hardness increased with the rising ball milling time due to work hardening.

Fogagnolo [56] produced aluminium alloy matrix composites with AlN and Si_3N_4 powders by low-energy ball milling. As shown in Figure 2-2, the apparent density decreased at first and then recuperated, followed by the stabilisation.

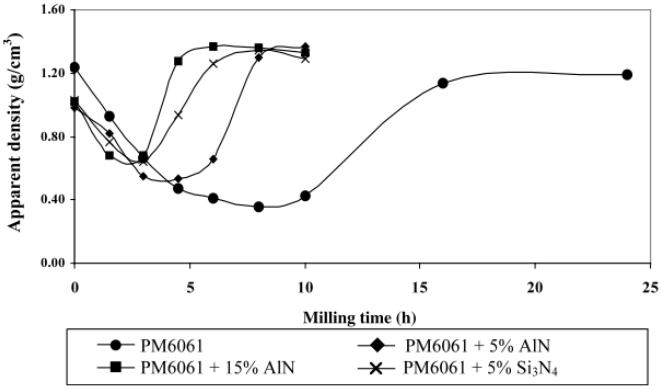

Figure 2-2 Apparent density vs. milling time.

Gan & Gu [57] investigated the compressibility of Cu/SiC_p , which was made by milling and compaction. It was found that both work hardening and the morphology of powders had major influence on the compressibility of powders, which was in accordance with Filho & Panelli [58].

Akbarpour & Alipour [47] produced copper and copper matrix composites reinforced with carbide nanoparticles by high energy ball milling and spark plasma sintering. It was found that the coefficient of friction and wear track depth were reduced through addition of 4 vol% SiC to copper matrix.

Fabrication of Cu and SiC nanoparticles was conducted via high energy mechanical milling and hot pressing in which effects of nanoparticle content were analysed [59]. It

was indicated that the main strengthening mechanism is Hall-Petch mechanism. Furthermore, Clyne approach was consistent with experimental data for predicting the strength of nano-size metal matrix composites.

Fathy et al. [60] fabricated Cu-Al_2O_3 composites by thermos-chemical technique, followed by cold pressing and sintering. It was found that compressive strength was increased by the increase of strain rate under room temperature. It was shown that Al_2O_3 nanoparticles could enhance the strength. There might be several relevant strengthening mechanisms: grain refinement, intermetallics phases, dislocation strengthening, Orowan strengthening and load transfer. Furthermore, cracks happened to the tested composite specimens before a compression of 50% in height.

AL-Mosawin et al. [61] synthesised the aluminium matrix composites reinforced by Al_2O_3 particles by uniball magneto-milling and uniaxial hot pressing. It was found that composite with more volume of Al_2O_3 particles (up to 10 vol.%) achieved higher compressive strength.

The tribological behavior of Cu/SiC composites was studied by Tjong & Lau [45], which was fabricated by hot isostatic pressing. It was found that the composite with up-to-20 vol.% could enhance the abrasive wear resistance, as seen in Figure 2-3. The improvement in wear resistance was attributed to SiC particles that reduced the degree of strain localization in the subsurface.

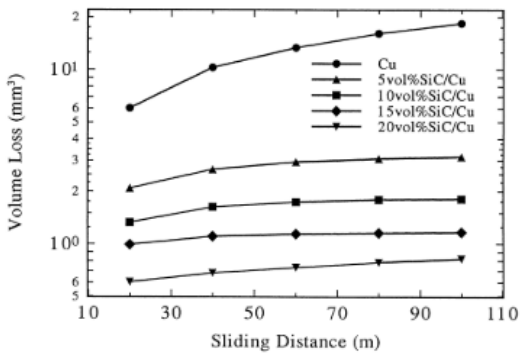

Figure 2-3 Volume loss vs. sliding distance.

The wear mechanism of copper matrix composite was also investigated by Safari et al. [62]. They used mechanical milling, cold pressing and spark plasma sintering to fabricate the composite. It was found that the delamination and abrasive wear were the dominant mechanisms in the wear test. The wear resistance rose up with the increase of reinforcement content to 5 wt%.

Moreover, microstructural development during fabrication and mechanical properties were investigated by Akbarpour et al. [63], which exhibited a compose in which non-random misorientation distribution and equiaxed nanograins with bimodal are mixed. It was shown that the grain structure of the copper matrix was refined while the fraction of low angle grain boundaries decreased. It revealed that high angle grain boundaries took a significant part in strengthening mechanism as well.

EI-Kady et al. [64] studied the thermal and electrical conductivity of A356/Al_2O_3 nanocomposites, made by squeeze casting and rheocasting. It was indicated that the thermal conductivity was reduced after the ceramic nanoparticles were added, reported in another research as well by Chu et al. [65]. Furthermore, the decrement happened to the electrical conductivity when the size was bigger that might be caused by the clustering of nanoparticles.

2.4 Metal matrix composites reinforced with graphene sheets

Nowadays, metal-matrix composites are widely employed in automobile aerospace applications. Among the promising reinforcements for MMCs, graphene, a recently discovered material, with two-dimensional platelet structure, consisting of carbon atoms, has attracted abundant attention from scientific communities.

Its unique physical and mechanical properties turn it into a promising nanofiller to

enhance mechanical, thermal and electrical properties of composites. Recent experiments exhibit that few-layered graphene nanoplatelets (GNPs) could be produced in large scale, indicating that large-quantities production cost is much lower [66, 67].

However, researches conducted on GNP are limited, attributed to a series of problems which are hard to distribute homogeneously for GNP and to obtain a full densification with metal powders as well as interfacial problems. Even so, early available results showed the matrix mechanical properties could been dramatically improved by introducing GNPs into Mg or Al matrix [68-70]. To date, there are a few researches about bulk graphene reinforced copper matrix composites [71-76]. Jagannadham [77, 78] deposited Gu/GNP films on Cu or other substrates. Zhang [79] deposited solution drops containing reduced Cu/GO (graphene oxide) on Cu films.

Guan et al. [80] added Cu-graphene powder to the melted Al, followed by stirring and cooling. A severe agglomeration of graphene was found, which could weaken the strengthening effect. Comparing to the hardness of pure Al, the hardness of the composite was increased by 40 %.

Bastwros et al. [81] fabricated the graphene reinforced Al 6061 composites by ball milling and hot compaction (in the semi-solid state). Compared to the Al 6061, the flexural strengths of the composites milled for 60 and 90 minutes were enhanced to 760 and 800 MPa respectively. It was reported that the carbide might form in the process, andthe dispersion of the graphene had effects on the strengthening effect.

Li et al. [82] used electrostatic interaction to combine the graphene oxide and aluminum powder to fabricate the graphene/aluminum composites. A homogenous distribution of reduced graphene oxide in the matrix was obtained through the method. Furthermore, the adsorption mechanism offered a way to get a 6 wt.% GO without agglomeration. Comparing to the unreinforced Al, hardness and elastic modulus were increased by 17

and 18%, respectively. The fabrication method provided a potential for a large-scale production of graphene/Al composites.

Yan et al. [83] combined ball milling and powder metallurgy to synthesise aluminum matrix nanocomposites reinforced with graphene. It was found that an effective distribution of graphene nanoflakes was obtained. Furthermore, the average yield strength and tensile strength were increased by 58 and 25 % respectively, compared to the aluminum alloy.

Li et al. [84] utilised cryomilling and hot extrusion to prepare the Al/Gr composites reinforced with different volumes of graphene nanoflakes (GNF). The ductility and strength were both increased over the monolithic aluminum. As shown in Figure 2-4 , agglomeration of graphene occurred when the content of GNFs was above 1.0 wt.%, which might be attributed to the big specific surface area and large aspect ratio of GNFs. Furthermore, the content of GNFs should not exceed than 4.0 wt.% through theoretical calculation.

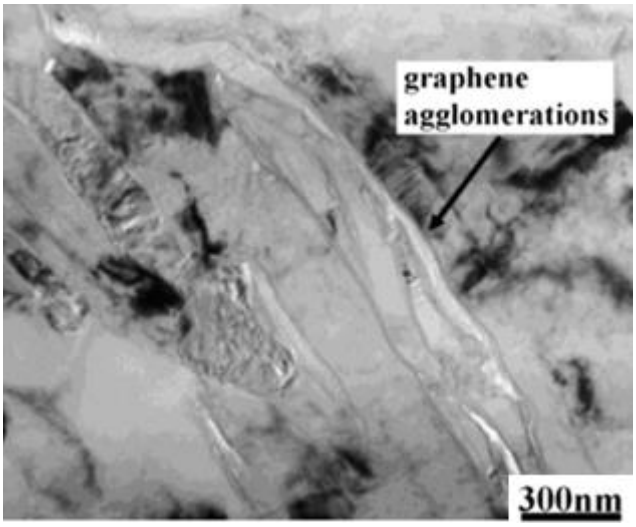

Figure 2-4 Bright-field TEM image showing graphene agglomerations.

Koltsova et al. [85] employed chemical vapor deposition to synthesise the new copper composite. As seen in Figure 2-5, the graphite/Cu composite was the most fragile, and

the fracture of the carbon nanofibers (CNF) /Cu composites became more viscous. The fracture of the graphene/Cu composites owned both fragile and viscous characteristics. Furthermore, the CNFs were thought to be the most appropriate material to enhance mechanical properties of Cu in the study, which had smaller grain size.

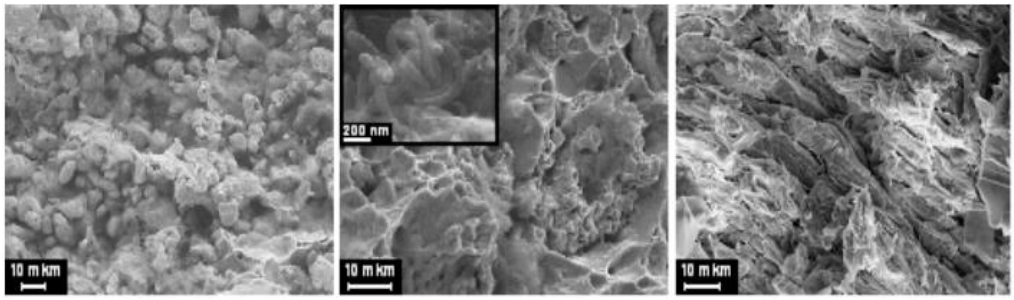

(a) (b) (c)

Figure 2-5 Fractures microphotography: (a) Cu-5% graphite, (b) Cu-5% CNFs and (c) Cu-3% graphene.

Kim et al. [86] utilised chemical vapor deposition (CVD) method to grow the graphene layers, and transferred the graphene layers to a substrate repeatedly. Copper-graphene composites obtained ultra-high strengths of 1.5 and 4.0 GPa for 70 and 100 nm repeat layer spacing respectively, which embodied the effective blocking effect of graphene on the metal-graphene interface.

Pavithra et al. [87] synthesised Cu-Gr composite foils through pulse reverse electrodeposition for the first time. It was reported that the graphene dispersed uniformly in the copper matrix, attributed to the optimized current density and pulse parameters. The strength was increased by about 96 % than that of pure Cu, and the elastic modulus (EM) was increased as well. Annealing was conducted as well after the fabrication of composites, indicating the graphene could inhibit the grain growth except the reinforcing effect.

Xie et al. [88] used the direct (one-step) electrochemical method to synthesise Cu/reduced graphene oxide composite films. It was found that the composite films had

a lower electrical resistivity than the polished Cu foil, which was probably ascribed to the rGO with higher conductivity. In general, the way afforded a new potential for the electrical contact materials.

Zhao & Wang [89] employed electroless plating process to prepare Cu/GNP composites, followed by consolidation and sintering. A homogeneous distribution of GNPs in the copper matrix was obtained, which was ascribed to the effect of precoating of Cu nanoparticles on GNPs. Moreover, there were 21 and 107 % increase in YM and TS respectively.

Bartolucci et al. [68] utilised ball milling, hot isostatic pressing (HIP) and extrusion to fabricate the graphene-aluminum nanocomposites. It was proved that multiwalled carbon nanotubes have enhanced the tensile strength of aluminium. However, it was indicated that the tensile strength and hardness of aluminium were lower due to the forming of aluminium carbide, which might be cause by the thermal exfoliation processing of graphite oxide.

Wang et al. [69] used the flake powder metallurgy to synthesise the aluminium matrix composites reinforced with graphene nanosheets. It was testified that 0.3 wt.% GNSs brought about 62 % increment of tensile strength compared to the Al matix, which was 249 MPa. Three strengthening mechanism were analysed to discuss the phenomenon, which were dislocation strengthening, grain refinement and stress transferring.

Lee & Han [72] investigated the multi-layer graphene (MLG) reinforced copper matrix composites, fabricated ball milling and rolling (HRDSR). There was enhancement in strength compared to the unreinforced copper matrix. The Orowan mechanism was the main strengthening mechanism.

It is found that measured density is no less than 98% of theoretical density [71, 72].

Nevertheless, when GNPs take a higher volume fraction, GNPs would tend to agglomerate, leading to a decrease of relative density of compacts [71]. Moreover, after ball milling, GNP defects have been indicated by Raman spectra. Surfaces and edges of graphene are damaged by repeated deformation, cold welding and fracture in the period of ball milling [71, 73, 90], and the grain of the Cu matrix is refined during ball milling, which is indicated by peak broadening in the XRD patterns [71]. There is no detectable oxide/carbide observed [71-73].

Hardness, yield strength (YS), ultimate tensile strength (UTS) and Young's modulus (E) of Cu-Graphene nanoplatelets could be improved when contents of GNP are no less than 8 vol.-% GNP [71-73, 76]. Nevertheless, decreased properties have been found because of inadequate dispersal of GNPs in the Cu matrix, which is fabricated through ultrasonication followed by sintering. So the authors decorate GNP with Ni, which has an improvement in bonding with the matrix and hinder agglomeration consequently [73].

Yue et al. [74] combined ball milling and hot pressing sintering to fabricate the graphene nanosheets (GNSs) reinforced copper matrix composites. It was indicated that the structure of GNSs could be broke if it has been milled for a long time. At the same time, the content of GNSs was a key index for the distribution for itself, which had influences on properties. When the content was lower than 0.5 wt.%, UTS could be improved. However, UTS began to decrease with an increase of the content of GNSs.

Tang et al. [75] decorated the graphene nanosheets with GNS-Ni hybrids by in situ chemical reduction method. Then the sonication was employed to mix copper powder and GNS-Ni hybrids, followed by hot pressing. It was found that the defects in the structure of graphene were elimated. Additionally, yield strength and Young's modulus were improved a lot by 1.0 vol% GNSs in this way, as displayed in Figure 2-6. The mechanical increase could be attributed to the high strength of intrinsic stiffness of GNS,

which could prevent shearing and rupture of composites.

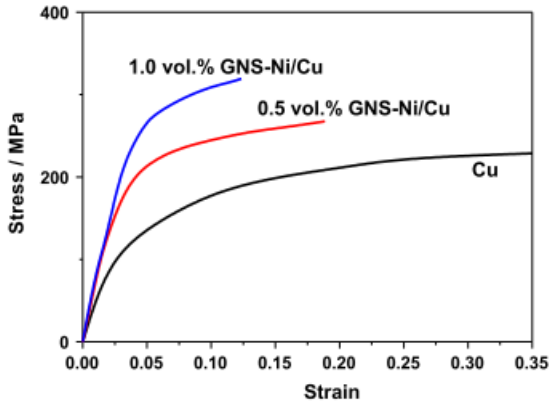

Figure 2-6 Tensile stress-strain curves of Cu and GNS-Ni/Cu.

Jagannadham [77, 78] employed tests of thermal conductivity on copper-graphene composites by vapor deposition. As shown in Figure 2-7, the cross plane and plane were investigated. As a result, the thermal conductivity of cross plane was reduced due to a lower thermal conductivity of graphene. However, the thermal conductivity in plane was not cut down by the thermal resistance of the interface. It turned out that random orientation was better to obtain bigger isotropic thermal conductivity. The same author also used different fractions of graphene in copper-graphene composites. It found that both the electrical conductivity and thermal conductivity were improved by a little volume fraction of GNP, which provided a new choice in the electro-friction materials and heat spreaders.

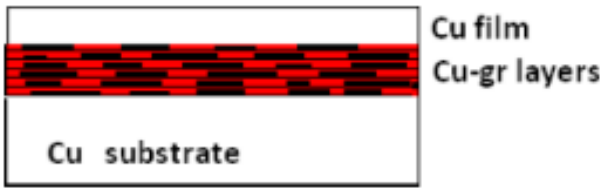

Figure 2-7 Schematic of Cu-graphene deposited on Cu substrate.

Jagannadham [91] employed the electrochemical deposition to synthesise the Cu-gr film as well. The rule of mixtures and effective mean field analysis were used to analyse the temperature coefficient of resistance and the electrical conductivity. It was found

that the resistivity of electrolytic Cu was decreased by 10-20 % when the volume of graphene was from 8-11 %.

2.5 Graphene/nanoparticles interaction: a road map to manufacture composites with exceptional properties

It has been found that manufacturing nanocomposites could bring about enhanced mechanical properties [92, 93]. Considering characteristics of graphenes, it could bring about new frontiers for the exploiting of nanoparticles, which could come true through synthesising nanoparticles and graphene.

Some researches, which is to decorate different nanoparticles of metal, metal oxides and semiconducting materials with two-dimension graphene, have been done and exhibit superior properties in the new composites [94, 95].

In view of molecular bonds are not required to connect graphene and nanoparticles, nanoparticles could be directly deposited on graphene sheets, which could lead to diminished detrimental effect of particles on the graphene substrate. Therefore, the way could provide a suitable room for nanoparticles to deposit on the graphene sheets, leading to novel functionalities for both graphene sheets and deposited nanoparticles. These properties could be applied in fields like catalytic, photo catalytic, optoeclectronics and energy storage [96, 97].

Lightcap et al. [97] utilised reduced graphene oxide and TiO_2 to produce a material that could be used as a catalyst nanomat, which certified the availability to fabricate composites with synergic properties including nanoparticles and graphene sheets.

Boostani et al. [98-102] employed ball milling and semi-solid processing to fabricate a new kind of aluminium matrix composites. SiC nanoparticles were dispersed properly

within the aluminium matrix capsulated by graphene sheets. During solidification, semi-solid stirring, ultrasonic treatment as well as pressure application were utilised.

Agglomeration of nano-size SiC particles was inclined to happen at grain boundaries rather than that at grain interior due to particle pushing mechanism through TEM investigations. There were two types of graphene sheets in which one was onion-like shells that encapsulate SiC particles and the other disk-shaped graphene nanosheets, attributed to the Orowan strengthening mechanism and the fiber pull-out mechanism respectively, due to the change of solidification mechanism. At the same time, the tensile strength and ductility had been improved by 45% and 83% respectively than that of the AR-SiC samples [99].

The processing route brought about large enhancement in properties of materials, which included 40% increase in thermal conductivity than pure SiC particle, decrease of repelling forces of SiC nanoparticles, 350% augment in yield strength and 258% enhancement in tensile ductility compared to the pure aluminum alloy, respectively, attributed to solidification alters from particle pushing to particle engulfment [98].

The same authors [102] investigated how the Hall-Petch, thermal enhanced dislocation, shear lag and Orowan mechanisms related to the composites as well. It was found that SiC nanoparticles were dispersed uniformly. Moreover, the analytical model demonstrated that the important roles of thermally dislocation and shear lag in strengthening the composite, ascribed to graphene sheets with an unusual negative thermal expansion coefficient. Furthermore, fractographic observations have shown that the transgranular fracture mode activated because of nao-void coalescence mechanism of the composites with graphene sheets related to prolonged ductility. The study also provided a possibility to enhance both ductility and tensile strength through the graphene encapsulating process [100].

2.6 Manufacturing processes of metal matrix nanocomposites

The production methods and properties of metal matrix composite materials reinforced with dispersion particles, platelets, noncontinuous (short) and continuous (long) [103]. As indicated in Figure 2-8, methods for fabricating MMCs are divided into three main categories. As for the liquid-state processing, casting and infiltration are the processes to obtain a high relative density. With respect to the solid-state processing, pressing and sintering is the common way to fabricate the composites. In order to avoid reactions in the well-bonded particle/fiber-matrix interface, the vapor-state processing is a good choice. On the other hand, high investment and low efficiency may be a big issue when the craft is considered.

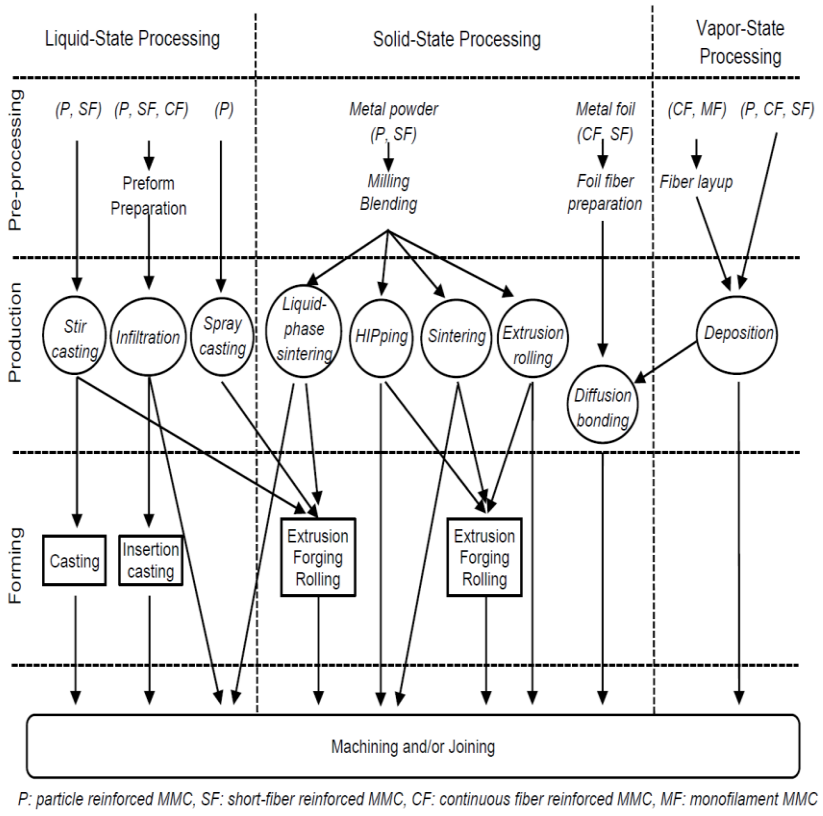

Figure 2-8 Processes of MMCs.

Nano-particles reinforced metal matrix composites, also called MMnCs, have been investigated for a couple of years, attributed to their promising properties for functional

and structural materials. In particular, mechanical properties, damping properties and mechanical strength could be improved. Nanocomposites are composites including at least one of the phased are in nano-size dimensions [36].

A main problem in producing MMcCs is the low wettability between the molten matrix and nano-particles. Currently, the alternative processes could be divided into two categories: in situ and ex situ. Usually ceramic nano-compounds could be generated during the in situ processes due to reaction, for instance the use of reactive gases. As for ex situ processes, a lot of techniques have been employed like powder metallurgy. Furthermore, ultrasound casting plays an assistant role in production.

There are some common ceramic compounds like SiC, Al_2O_3, ZnO [33] used for reinforcement of Al, Cu, Mg, and other materials [104] by which microhardness, electrical conductivity and wear resistance could be enhanced.

For a large-scale production of MMnCs, the main concern is the low wettability for nano-particles. In order to solve the low wettability, many processes have been studies and used. Basically, they could be classified into three kinds: liquid processes, semisolid processes and solid processes.

2.6.1 Liquid processes

Allahkaram et al. [33] utilised the direct current and pulse current plating to accomplish the composite coating. It was found that a finer grain size was achieved in the Al_2O_3 reinforced copper matrix composite. Comparing to direct current (DC) composite coatings, pulse current (PC) ones were more coherent. The minimum thickness of PC samples was more than ones of DC.

It was demonstrated that Al_2O_3 nano-particles were distributed uniformly in the Mg matrix by a stir-casting method [93]. The grain structure was refined, and the CTE

decreased. Furthermore, there were obvious enhancement in both tensile properties and hardness. For the strength mechanism, CTE mismatch was found most effective among all the mechanisms.

Kang & Kang [105] utilised the plasma-sprayed method to make a mixed SiC/Cu matrix composite. After ball milling and sieving, the mixed powder was plasma-sprayed onto a graphite substrate in air. It was detected that a lot of cuprous oxides occurred in the compositions through XRD analysis, which was indicated in Figure 2-9. Furthermore, most pores were detected near the SiC and it was discovered micropores on the surface of SiC, attributed to the thermal expansion and the decomposition of SiC.

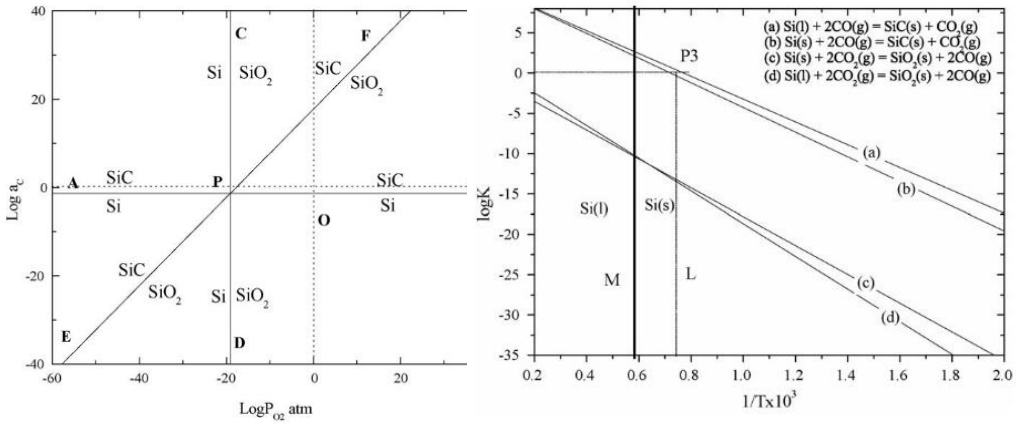

Figure 2-9 Phase stability diagram for Si-C-O at 1680 K & the equilibrium constant vs. temperature (K).

Lan et al. [106] fabricated the AZ91D magnesium composites reinforced with SiC nanoparticles by ultrasonic method. It was found that SiC nanoparticles were almost distributed uniformly in the matrix. Additionally, microhardness of the composites was enhanced with the increase of percentage of SiC. At the same time, partly oxidisation and SiO_2 were found through energy-disperse X-ray spectroscopy (EDS) and X-ray photoelectron spectroscopy (XPS).

As displayed in Figure 2-10, Zhu et al. [107] utilised a electroforming to fabricate Cu/SiC_p composites. It was found that the hardness and bend strength of Cu/SiC_p

composites rose with the increase of SiC_p. Compared to these properties, the conductivity factor and CTE showed an opposite trend as SiC_p content increased. In addition, it was detected that smaller SiCp had a bigger content than that of larger ones.

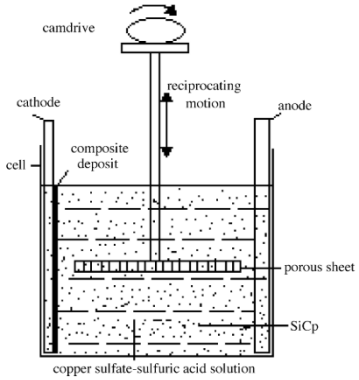

Figure 2-10 Equipment of electroforming.

2.6.2 Solid processes

Among the solid processed, PM techniques were the most employed method, which used ball milling, sintering and other crafts. Moreover, a lot of powder metallurgical experiments have been applied to fabrication and improvement of new materials. PM involves three main parts of the deformation of particle, which are fracturing, welding and repeated deformation.

Kollo et al. [108] utilised aluminium and SiC to fabricate the SiC_p/Al nanocomposites through ball milling and hot pressing. In the process of ball milling, stearic acid was usually added as a process control agent (PCA), which had a huge effect on the morphological evolution of composites. In addition, it was indicated that heptane could enhance the effects of welding of powders. The energy transferring reduced with an increase of balls at low filling levels, and smaller diameters of balls introduced the biggest input energies.

Tavoosi et al. [109] ball-milled the aluminium and ZnO powders to fabricate the Al-

Zn/α-Al_2O_3 nanocomposite and then annealed the composites. It was found that the increased microhardness of the composites might be caused by the decrease of crystallize size, formation of Al-Zn and Al_2O_3.

Barmouz et al. [110] employed the friction stir processing (FSP) to fabricate copper matrix composites reinforced with nano-sized and micro-sized SiC particles. It was found that grain of nano-sized nanoparticles was finer than that of the micro-sized ones. Furthermore, the percent elongation and the tensile strength were lower than the ones without powder. On the other side, the yield strength was increased. The effect of nano-sized particles was more obvious than that of micro-sized particles. Additionally, there was an enhancement in the wear resistance with the increase of volume fraction for both the two kinds of particles.

It was proved by Efe et al. [111] that the SiC particle size had effects on the Cu-SiC composites. PM and hot pressing sintering were utilised in the research. Especially, there were twice pressing before the sintering and after that, making the samples take shape and become more compacted. Through the verification of XRD, EDS, a high density was achieved through the method at a lower sintering temperature. In addition, hardness, relative density and electrical conductivity were enhanced with the increasing sizes of SiC particles, making the material a promising alternative in the electrical components.

Güler & Evin [112] employed a different way to fabricate the copper composites, combined of mechanical alloying (MA), cold pressing, sintering and forging. Four kinds of oxides were used as reinforcements at different ratios. It was displayed that 4 wt.% oxides exhibited the most superior electrical conductivity relatively. Furthermore, less weight loss was concluded for the composite reinforced by a 4 wt.% ZnO from which the best electrical conductivity was achieved as well.

As displayed in Table 2-1, advantages of disadvantages of most common techniques of fabricating MMnCs are shown [36].

Table 2-1 Fabrication methods for MMnCs.

Process	Advantages	Limitations
Spray Pyrolysis	Effective preparation of ultra fine, spherical and homogeneous powders in multicomponent systems, reproductive size and quality.	High cost associated with producing large quantities of uniform, nanosized particles.
Liquid Infiltration	Short contact times between matrix and reinforcements; moulding into different and near net shapes of different stiffness and enhanced wear resistance; rapid solidification; both lab scale and industrial scale production.	Use of high temperature; segregation of reinforcements; formation of undesired products during processing.
Rapid Solidification Process (RSP)	Simple; effective.	Only metal-metal nanocomposites; induced agglomeration and non-homogeneous distribution of fine particles.
RSP with ultrasonics	Good distribution without agglomeration, even with fine particles.	
High Energy Ball Milling	Homogeneous mixing and uniform distribution.	
CVD/PVD	Capability to produce highly dense and pure materials; uniform thick films; adhesion at high deposition rates; good reproducibility.	Optimization of many parameters; cost; relative complexity.
Chemical Processes (Sol-Gel, Colloidal)	Simple; low processing temperature; versatile; high chemical homogeneity; rigorous stoichiometry control; high purity products.	Weak bonding, low wear-resistance, high permeability and difficult control of porosity.

2.6.3 Semisolid processes

Bastwros et al. [9] utilised the ball milling technique to synthesise Al6061 composite reinforced by 1.0 wt.% graphene. The graphene exfoliated from graphite and Al6061 were milled and then consolidated at room temperature and semi-solid regime twice. There was an increasement for strength according different milling times. Furthermore, graphene was dispersed uniformly and the stacked layers were reduced with further milling, as displayed in the scanning electron microscopy (SEM) images (Figure 2-11) of fracture surfaces.

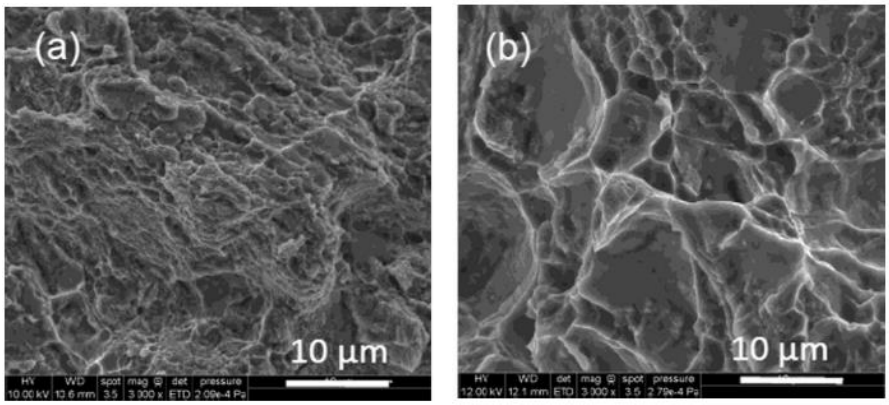

Figure 2-11 SEM images of fracture surfaces: (a) Al6061-1.0 wt.% with milling time of 90 min, and (b) unalloyed Al6061 with a milling time of 90 min.

EI-Kady et al. [64] combined the rheocasting and squeeze casting techniques to fabricate A356/Al_2O_3 nanocomposites. The A356 alloy was cooled down to a semisolid temperature and then stirred. After preheated Al_2O_3 nanoparticles were added into the molten alloy, the mixed materials were poured into a preheated tool steel mould and then squeezed by a hydraulic press. As shown in Figure 2-12, the thermal conductivity began to decrease due to the clustering of reinforced nanoparticles.

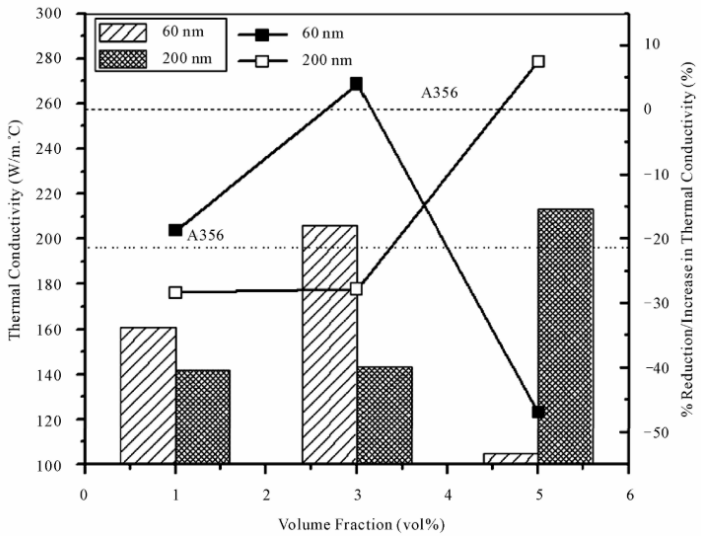

Figure 2-12 The average thermal conductivity with volume fraction of of Al2O3.

Nie et al. [113] synthesised SiCp reinforced AZ91 composites by semisolid stirring assisted with ultrasonic vibration. It was found that the ultimate tensile strength and yield strength were improved with the increase of extrusion temperature, as indicated in Figure 2-13. It showed a same trend with the decrease of the stirring time.

Furthermore, grain of matrix was refined when the temperature increased. What's more, the SiC bands were decreased with the increase of extrusion temperature.

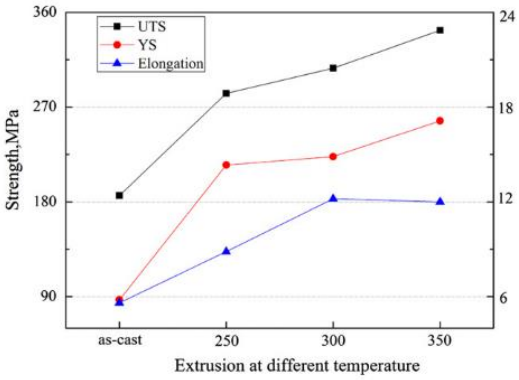

Figure 2-13 Tensile strength at different temperature.

Boostani et al. [98, 99] employed the semisolid casting to fabricate aluminium matrix composites reinforced by graphene encapsulated silicon carbide nanoparticles, assisted with ball milling and non-contact ultrasonic vibration. The innovative method made use of the promising properties of graphene like high thermal conductivity. The method changed the solidification mechanism from the pushing mechanism to engulfment mechanism. As displayed in Figure 2-14 (a), the particles were less than 1 μm after ball milling, which was good to obtain better dissolution. Additionally, a homogeneous distribution was achieved, as indicated in Figure 2-14 (b). Accordingly, there was an augment in the tensile properties and tensile ductility.

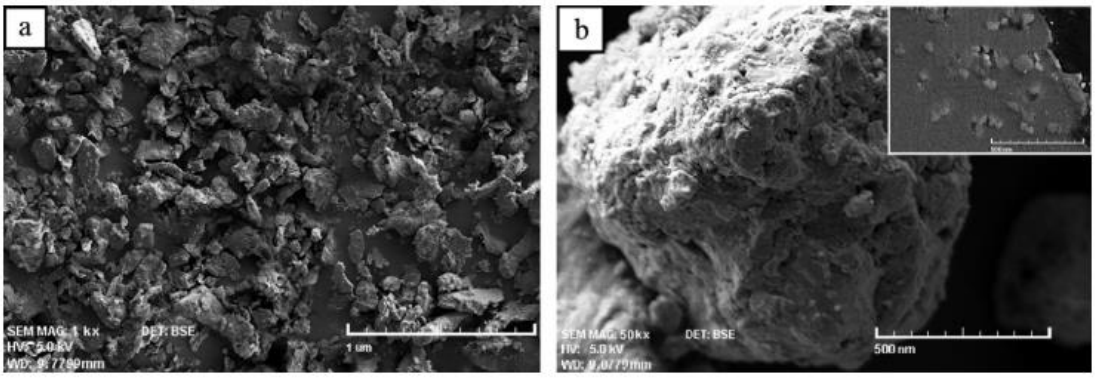

Figure 2-14 (a) Morphology of mixed powder, and (b) high magnification image of (a).

Selective laser melting was utilised to fabricate the Ti matrix nanocomposites reinforced with TiC nanocrystalline [114]. The TiC reinforcement was quite different form the particulate morphology at beginning, as shown in Figure 2-15. The elastic modulus and dynamic hardness increased respectively than those for the unreinforced Ti sample.

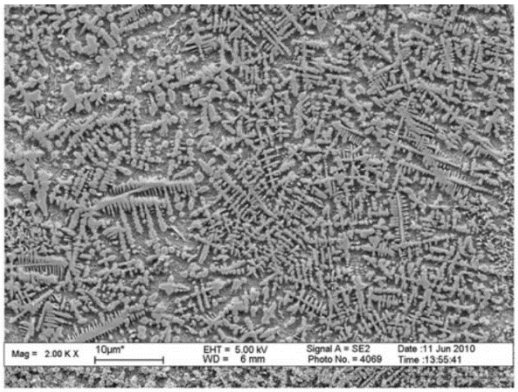

Figure 2-15 FE-SEM images of TiC/Ti nanocomposites.

2.7 Strengthening mechanisms of MMnCs

There are four strengthening mechanism contributing to the superior mechanical properties of metal matrix composites reinforced with nanoparticles, including load transfer effect, Hall-Petch strengthening, Orowan strengthening, and CTE (coefficient of thermal expansion and EM (elastic modulus). These methods will be clarified below separately.

2.7.1 Load transfer effect

The load transfer means that load transfers from the soft and compliant matrix to the stiff and hard particles under an applied external load, contributing to the strengthening of the base material. A modified Shear Lag model (Equation (2-1)) put forward by Nardone & Prewo [115] is commonly employed to predict the contribution in strengthening attributed to load transfer of particulate-reinforced composites [116-118]:

$$\Delta\sigma_{LT} = v_P\sigma_m\left[\frac{(l+t)A}{4l}\right] \quad (2\text{-}1)$$

where v_P is the volume fraction of the particles, σ_m is the yield strength of the unreinforced matrix, *l* and *t* are the size of the particulate parallel and perpendicular to the loading direction, respectively. With respect to equiaxed particles as reinforcements, Equation (2-1) is modified to Equation (2-2):

$$\Delta\sigma_{LT} = \frac{1}{2}v_P\sigma_m \quad (2\text{-}2)$$

2.7.2 Hall-Petch strengthening

Considering dislocation movement could be hindered by the grain boundaries, the grain size affected the metal strength strongly. It is attributed to the large lattice disorder characteristic and the different orientation for adjacent grains in these regions, which prevent the moving of dislocations in a continuous slip plane. The Hall-Petch equation (Equation (2-3)) involves the average grain size and the strength [119]:

$$\Delta\sigma_{H-P} = \frac{k_y}{\sqrt{d}} \quad (2\text{-}3)$$

where k_y means the strengthening coefficient (which is the characteristic constant of each material).

As for the final grain size of metal matrix composites, particles play an essential part due to their interaction with grain boundaries, serving as pinning pointing to prevent their growth. As indicated in the Zener equation (Equation (2-4)) [118], a finer structure could be caused by the decrease of d_P and the increase of v_P:

$$d_m = \frac{4\alpha d_P}{3v_P} \quad (2\text{-}4)$$

where d_P stands for particle diameter, v_P stands for volume fraction and α stands for a proportional constant.

2.7.3 Orowan strengthening

The Orowan mechanism refers to the interaction of dislocations and nanoparticles [119]. To be specific, under the external load, the non-shearable ceramic nanoparticles as reinforcement would fix the crossing dislocations and facilite the bowing of dislocations around the particles, which is called Orowan loops. The expression (Equation (2-5)) for the Orowan strengthening is below:

$$\Delta\sigma_{OR} = \frac{0.13bG}{d_P(\sqrt[3]{\frac{1}{2}v_P}-1)}\ln(\frac{d_P}{2b}) \tag{2-5}$$

where G stands for the matrix shear modulus and b stands for the Burger's vector.

2.7.4 CTE and EM mismatch

The mismatches between reinforcement particles and the metal matrix in CTE (coefficient of thermal expansion) and EM (elastic modulus) is accommodated through material cooling and straining by GNDs (the formation of geometrically necessary dislocations).

The following expressions can be used to estimate the GND densities caused by CTE (Equation (2-6)) and EM (Equation (2-7)) [118]:

$$\rho^{CTE} = \frac{A\Delta\alpha\Delta T v_P}{bd_P(1-v_P)} \tag{2-6}$$

$$\rho^{EM} = \frac{6v_P}{\pi {d_P}^3}\varepsilon \quad (2\text{-}7)$$

where A stands for the geometric constant, ΔT stands for the difference between temperatures of processing (or heat treatment temperatures) and the test. In addition, the combined strengthening owing to the mismatch of CTE and the mismatch of EM can be calculated through the Taylor equation (Equation (2-8)) [120]:

$$\Delta\sigma_{CTE+EM} = \sqrt{3}\beta Gb\left(\sqrt{\rho^{CTE}} + \sqrt{\rho^{EM}}\right) \quad (2\text{-}8)$$

where β is a constant.

2.7.5 Sum of contributions

One expression (Equation (2-9)) to evaluate the strength of composites, σ_c, is to add the initial yield strength of the unreinforced matrix, σ_m, with the contributions correlated with all the different strengthening effects, $\Delta\sigma_i$, as:

$$\sigma_c = \sigma_m + \sum_i \Delta\sigma_i \quad (2\text{-}9)$$

There are some alternative ways proposed in some studies to evaluate σ_c, taking into account the superposition of all the effects [117, 121]. It is suggested that σ_c (Equation (2-10)) could be calculated through making the root of sum of squares including all the strengthening effects:

$$\sigma_c = \sigma_m + \sqrt{\sum_i \Delta{\sigma_i}^2} \quad (2\text{-}10)$$

Chen & Zhang [116, 117] proposed one method (Equation (2-11)) to evaluate the strength, considering the CTE mismatch (Equation (2-12)), Orowan strengthening (Equation (2-13)) mechanism and load-bearing effect, as:

$$\sigma_c = (1 + 0.5v_P)\left(\sigma_m + A + B + \frac{AB}{\sigma_m}\right) \quad (2\text{-}11)$$

$$A = 1.25G_m b\sqrt{\frac{12\Delta\alpha\Delta T v_P}{bd_P(1-v_P)}} \quad (2\text{-}12)$$

$$B = \frac{0.13G_m b}{d_P\left[\left(\frac{1}{2v_P}\right)^{\frac{1}{3}}-1\right]}\ln\frac{d_P}{2b} \quad (2\text{-}13)$$

where A stands for CTE mismatch and B is related to Orowan effect.

2.8 Summary

Among all the metal matrix composites, copper matrix composite is unique for its application in contactor, heat sink, electronic package and so on, attributed to its high electrical and thermal conductivity, wear resistance, and other superior properties. In addition, SiC, Al_2O_3 and some other kinds of ceramic particles as reinforcement could enhance the hardness of composites.

As for reinforced particles, large-size particles may cause a few problems like cracking and low ductility. On the other side, nanoparticles exhibit novel and superior properties due to their nanoscale size. However, there is still difficulty in distributing nanoparticles in the matrix uniformly.

Considering the fabrication process, powder metallurgy has been utilised to fabricate nanoparticles reinforced copper matrix composites, which could reduce CTE of composites. Furthermore, SiC_P reinforced copper matrix composites have receive wide attention for their good mechanical properties, high thermal conductivity, high melting point and low costs, as an ideal electrical contact material.

In term of graphene, it has attracted a lot of attention due to its unique two-dimensional platelet structure and unusual physical and mechanical properties. To date, there are some researches around Cu-Graphene, reveals that graphene can improve hardness, YS, UTS and so forth.

On its combination with ceramic matrix composites, graphene can hinder ceramic grain from growing. Furthermore, fracture toughness, flexural strength and other properties have been enhanced by adding graphene into the ceramic matrix [31]. Moreover, decorating nanoparticles with graphene has shown a promising application in fields like catalytic and photo catalytic. Some studies have indicated that aluminium graphene sheets encapsulating SiC nanoparticles exhibits an improvement in tensile ductility [98, 99].

Therefore, graphene could be applied to copper matrix composites reinforced with nanoparticles, solving the agglomeration of nanoparticles and enhancing properties of traditional copper matrix composites.

Chapter 3 Experimental methodology

3.1 Sample preparation

3.1.1 Ball milling

The planetary mono mill used in the experiment is made by Fritsch GmbH in Germany, as shown in Figure 3-1. The movement of its vial is planetary, which is the reason it owes the name. In addition, the vial rotates around its own axis. The position of the supporting disk must be adjusted to achieve the balance between the vial with different quantities of material and itself. Furthermore, the centrifugal forces induced by the vial and the supporting disk both have effects on the vial contents [122].

Figure 3-1 Fritsch pulverisette 6 planetary mono mill.

In this study, commercially atomized Cu powder (spherical, 99.9 wt% purity; average particle size 30 μm, HTNANO), SiC powder (average particle size 50 nm; purity 99.9%, NANOINGLOBAL) and graphene nanoplates (diameter: 5-10 μm and thickness: 3-10 nm, XFNANO) were used in experiments. The chemical composites of copper powder are displayed in Table 3-1:

Table 3-1 Chemical composites of as-received copper powder.

Element	Cu	Al	Ca	Mg	Fe	Mn	Na	Co
wt. %	99.9	0.002	0.01	0.001	0.001	0.001	0.001	0.001
Element	Si	Ni	Pb	K	N	C	S	O
wt%	0.001	0.001	0.001	0.001	0.001	0.01	0.001	0.08

There are four kinds of materials: pure as-received copper, pure milled copper, copper with 4 vol% SiC and copper with 4 vol% SiC and 1 vol% GNP. Mechanical milling was performed in a planetary ball mill under an argon atmosphere at room temperatures for different ball milling times. The ball-to-powder ratio was 8.5:1, and 1 wt.% stearic acid was used as a process control agent. The longest ball milling time was 20 h to investigate the change of microstructure and morphology. Moreover, the specific setting of processing parameters is displayed in Table 3-2.

Table 3-2 Parameters of ball milling.

Processing parameters setting	
Filling quantity and material of grinding bowl	80ml, stainless steel
Diameter and material of grinding balls	5mm, stainless steel
PCA	Stearic acid
Atmosphere	Argon
Milling modes	Forward and reverse
Rotational speed	200 revolutions per minute (rpm)
Time of running and pause per cycle	5min, and 15min respectively

3.1.2 Cold pressing and sintering

Prior to sintering, the mixed powder was cold pressed at room temperature in a uniaxial steel die by the 10 tonne hydraulic press with an inner diameter 10 mm below, at 850

MPa on both sides for 5 min respectively, as shown in Figure 3-2 (a). Then green pellets had dimensions with 10 mm in diameter and 3-5 mm thickness. The principle of cold welding was to weld materials together in a solid state without heating or fusion. Before the pressing, the die was sprayed with dry Polytetrafluoroethylene (PTFE) as a lubricant for reducing friction between the stamp and die. Furthermore, one graphite sheet was put under powder on one side to prevent the leaking of powder, and it could also make the removal of samples easier. The schematic diagram of die is displayed in Figure 3-2.

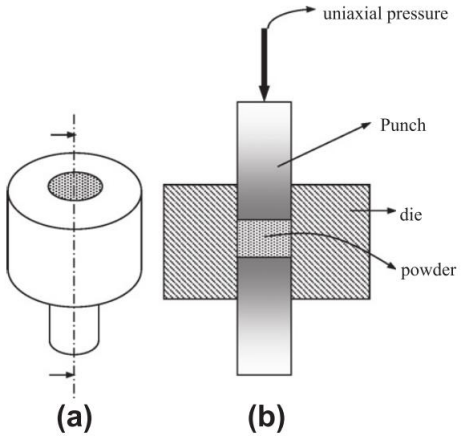

Figure 3-2 Schematic of dies.

After pressing, the samples were put into a ceramic and then pushed into the middle of the tube furnace, which was displayed in Figure 3-4 (b). As displayed in Figure 3-3, at the first stage, the consolidated nanocomposites were degassed at 400 ºC for 1 h under argon atmosphere and atmospheric pressure (the melting point of stearic acid is 400 ºC). It was suggested that a degassing procedure could improve the sintering [23]. Then, the sintering was conducted at 700, 750, 800 ,850, and 900 ºC for 2 h, and the heating rate was 10 ºC/min. The air cooling was used right after heating.

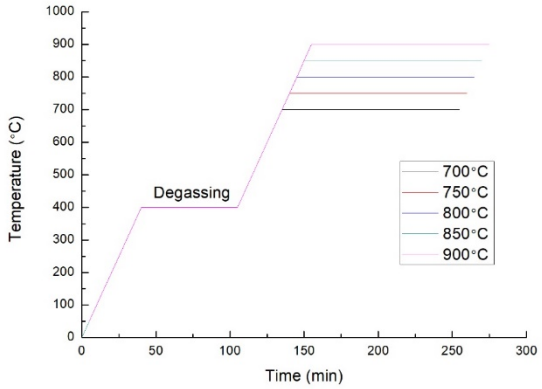

Figure 3-3 Heating curve of sintering.

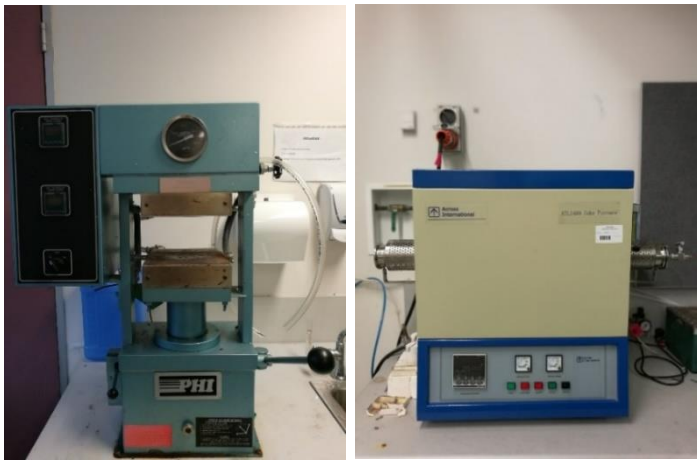

(a) (b)

Figure 3-4 (a) 10 Tonne hydraulic press and (b) KTL 1400 tube furnace.

3.2 Experiment and analysis

3.2.1 Hot mounting, grinding and polishing

As shown in Figure 3-5, specimens were hot mounted to a dimension with a diameter of 30 mm, which suit the holder of the polishing machine. In this case, a 22.5 ml multi-fast powder was used for mounting. The mounting temperature was 180 ºC, and the water cooling was conducted.

Figure 3-5 Struers citopress 20 hot mounting.

Struers TegralPol-21 automatic grinding/polishing machine was used in the polishing, as displayed in Figure 3-6. Considering the hardness and materials of samples, an appropriate procedure for grinding and polishing was chosen from the database of the console. First, samples were grinded by #800 SiC foil and then by a 9-µm MD-largo surface, followed by the 3- µm and 1- µm MOL surfaces. Finally, the MD-Chem surface was utilised. In addition, an optical microscope was used to examine the result of polishing.

Figure 3-6 Struers TegralPol-21 automatic grinding/polishing machine.

3.2.2 KEYENCE laser microscope (3D & profile measurement) and density measuring instrument

The morphology of sintered samples was initially observed by the laser microscope as displayed in Figure 3-7 (a). Unlike the common optical microscope, the laser microscope could be used to analyse and characterize the 3D surface of specimens. Specimens were scanned in XYZ directions to collect the detailed height information. As a result, a large depth of field, high-resolution, color image could be obtained.

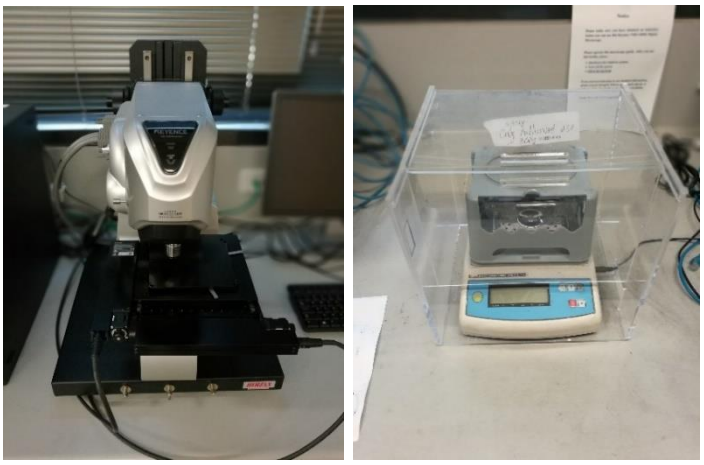

(a) (b)

Figure 3-7 (a) KEYENCE laser microscope and (b) automatic density measuring instrument.

As indicated in Figure 3-7 (b), the density of sintered preforms was calculated by measuring the weight of samples in air and the other one in water, on basis of Archimedes principle. First, the weight of samples in air was measured. Then it was put on the inner platform to measure full of stilled water for the second measurement. Then the actual density could be calculated by the instrument. The error of data in the measurement was kept within 1%. Every group of samples were measured three times and the average value was taken as the density.

3.2.3 X-ray diffraction

As displayed in Figure 3-8, all powders were characterised by the GBC MMA XRD, with the Cu Kα radiation (Kα =1.5405 Å) and a current of 28.4 mA and an accelerating voltage 35 kV. The scanning rate was 2 °/min and the step size was 0.02 °. Scanning angle ranged from 20° to 100°. Then the data was processed by Jade and TRACES softwares.

Figure 3-8 GBC MMA XRD.

Furthermore, the lattice strain and average crystallite size could be calculated thorough the line profile analysis of XRD peaks [123]. During ball milling of different time, XRD peak broadening would occur. There are three main methods to calculate crystallite size including Scherer's formula, Williamson-Hall formula and Warren-Averbach formula. In this study, Williamson-Hall method was utilised to calculate the crystallite size because it is simple and suitable. Therefore, it can be expected from the following W-H equation:

$$\beta_{hkl} \cos \theta_{hkl} = \left(\frac{K\lambda}{t}\right) + 4\varepsilon \sin \theta_{hkl} \quad (3\text{-}1)$$

where β_{hkl} stands for FWHM (the full width at half-maximum), θ_{hkl} means the Bragg angle (°), K stands for the shape factor of 0.9, λ is the X-ray wavelength (1.5406 Å), t means the effective crystallite size (nm), ε is the lattice strain. Then a liner plot of $\beta_{hkl} \cos \theta_{hkl}$ against $4 \sin \theta_{hkl}$ should be made to determine the lattice strain and

crystallite size. The crystallite size and strain could be calculated from the intercept and slope respectively.

3.2.4 Microhardness testing

The microhardness is related to the elastic stiffness, strength, plasticity, ductility and toughness. In this study, indentation was adopted to test the Vickers hardness, which was to estimate the resistance of material deformation. The standard indentation is displayed in Figure 3-9, based on two dimensions of an indentation. The hardness is calculated by the indentation area and the load, which could be converted into pascals. The hardness value is calculated based on the formula below:

$$HV = \frac{F}{A} \approx \frac{1.8544F}{d^2} \tag{3-2}$$

The unit of the force of indentation (F) is the kilogram, and d is the indented diameter for the area. The surface area A could be converted below:

$$A = \frac{d^2}{2sin68^\circ} \tag{3-3}$$

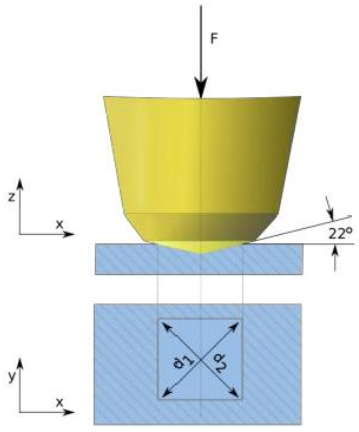

Figure 3-9 Schematic of the indenter and indentation of vickers hardness.

After grinding and polishing, the microhardness of samples was measured by the TIME TH7 15 microhardness tester, with a load of 0.98 N and a dwelling time of 10 s, as shown in Figure 3-10. On accountant of accuracy, 15 effective places of the polished surface were indented and measured through which Vickers hardness was acquired directly. The relative error between the two dimensions was kept within 5%. The criteria is as follows:

$$\frac{|D_1 - D_2|}{D_1} < 5\% \tag{3-4}$$

Figure 3-10 TIME TH7 15 microhardness tester.

3.2.5 Field emission scanning electron microscopy

As displayed in Figure 3-11, the morphological of powders and the morphological evaluation of powder samples were analysed through the JEOL JSM-7500FA field emission scanning electron microscope (FESEM) using at 9.5 mA and 5 kV. The FESEM is equipped with a 30 kV in-lens cold field emission gun possessing 1.4-nanometer spatial resolution. Because the FESEM may access superior image quality at 0.1kV, charging effects on materials could be reduced. Thus it is suitable for scanning thin foils and nanosized materials embedded on the thin support film. In this study, powder must be coated with thin layer to make it conductive for current since the

FESEM works with electron. Furthermore, a high vacuum must be sustained.

Figure 3-11 JEOL JSM-7500FA field emission scanning electron microscope (FESEM).

3.2.6 Compression test

As indicated in Figure 3-12, the compression tests of sintered samples were performed by the 500 KN Instron universal testing machine. The maximum displacement was kept close to 50% of the specimen height. The load rate was 0.004 mm/s. The dimension of samples were (2 ± 0.05) mm in diameter and (5 ± 0.05) mm in length (L/D = 2.5), which was based on standard requirements [124, 125]. Moreover, three samples were prepared for the same compression test to keep the accuracy of results. The compressive yield strength was calculated by the 0.2% offset principle [126].

Figure 3-12 500 KN Instron universal testing machine.

Chapter 4 Effect of sintering temperature

4.1 Introduction

In this study, pure copper and Cu-SiC-GNP (milled for 2 h) are utilised to analyse the influence of sintering temperature. Microstructure, morphology, density and microhardness are investigated to find out the correlation between the performance and sintering temperatures.

4.2 Experimental procedure

Commercially atomized Cu powder (spherical, 99.9 wt% purity; average particle size 30 μm, HTNANO), SiC powder (average particle size 50 nm; purity 99.9%, NANOINGLOBAL were used in experiments. As for Cu-SiC-GNP composites, SiC and GNP take up 4 vol % and 1 vol % respectively. pure copper and Cu-SiC-GNP (milled for 2 h) were compacted with 850 MPa in a steel mold of 10 mm in the inner diameter. Three specimens were used in every single fabrication and test of materials in consideration of accuracy. Then the sintering was conducted under the argon atmosphere in a tube furnace at a range from 700 to 900 ºC for 2h with the heating rate of 10 ºC/min, followed by air-cooling. Afterwards, microhardness, relative densities were measured, and microstructure was observed.

4.3 Results and discussion

4.3.1 Pure copper

4.3.1.1 Optical images

Optical microstructures of pure copper samples sintered at 700, 750, 800, 850 and 900 ºC are displayed in Figure 4-1. Light areas were copper matrix and dark areas were

porosity. It could be found that grains of samples sintering at 700 and 750 ºC are distributed independently and grain boundary could be observed clearly. When temperature rose to 800 ºC, grains became bigger and connected with other grains so that grain boundary was hard to distinguish. At the same time, the proportion of pore turned bigger and a few of big voids began to occur, especially at 900 ºC.

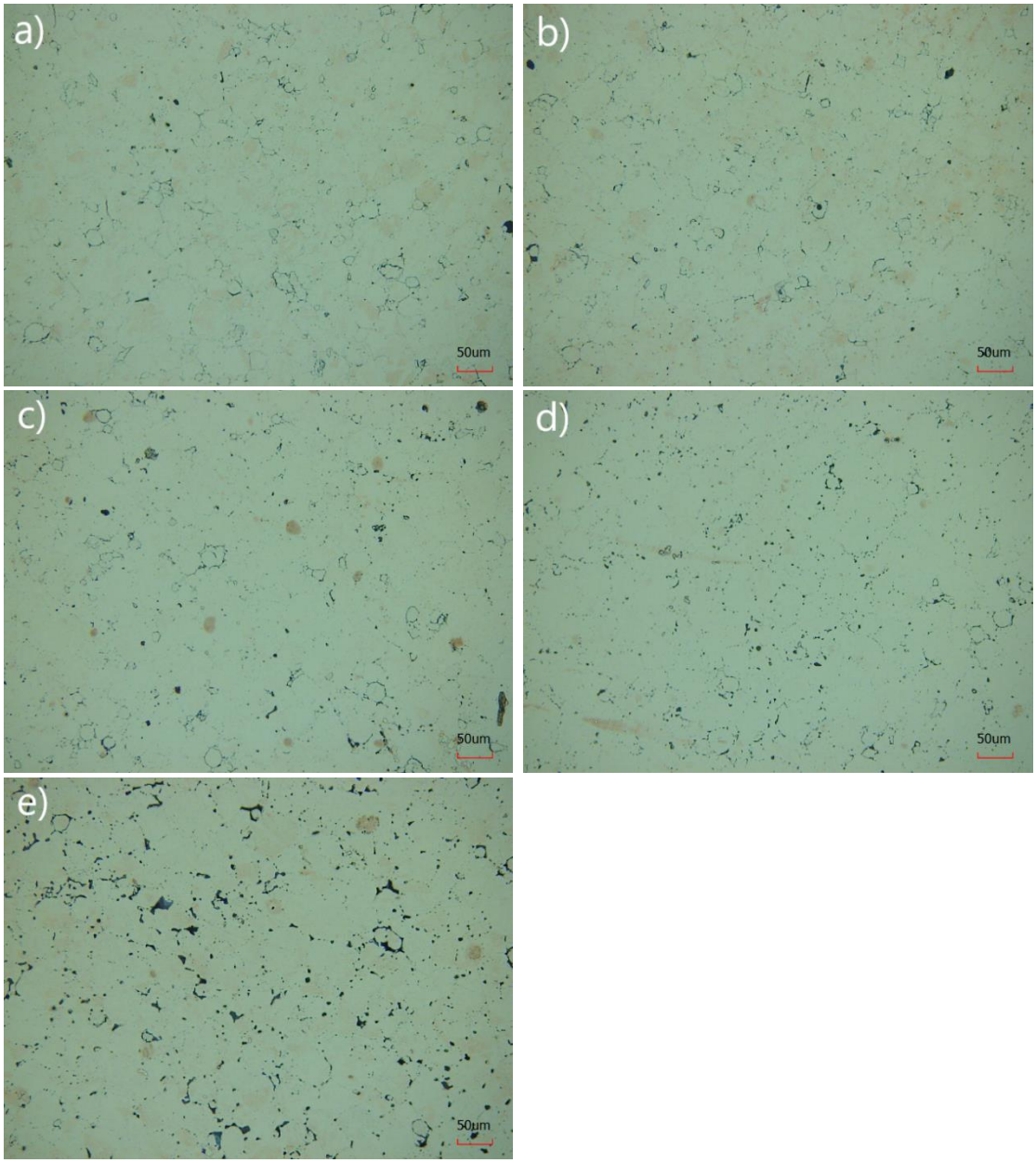

Figure 4-1 Optical micrographs of pure copper samples sintered at (a) 700 ºC, (b) 750 ºC, (c) 800 ºC, (d) 850 ºC and (e) 900 ºC.

4.3.1.2 Density measurement

It was illustrated that density of specimen changed when sintering temperature went up in Table 4-1 and Figure 4-2. There was a tiny decrease when temperature increased to 750 ºC. At 800 ºC, density ascended to the maximum, which might be attributed to the enhanced connectivity of grains. It could be seen that grains became bigger and grain boundaries could not be seen clear, and the porosity level was reduced to the minimum. After the sintering temperature increased to 850 ºC, the density decreased. It decreased to the minimum at 900 ºC due to the increase of pore and void. The error of density showed that counting statistics at 700 and 850 ºC were slightly poorer than that in other temperatures in the density measurement [127].

Table 4-1 Density of samples made of the as-received copper powder.

Temperature (ºC)	Theoretical density (g/cm^3)	Relative density (%)	Porosity (%)
700	8.44	94.1%	5.9%
750	8.41	93.9%	6.1%
800	8.53	95.2%	4.8%
850	8.45	94.35%	5.65%
900	8.18	91.3%	8.7%

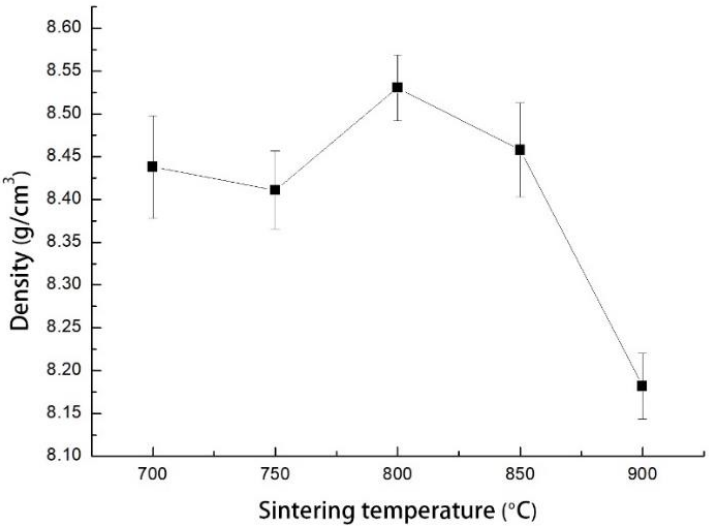

Figure 4-2 Density of as-received copper powder compacted in 850 MPa vs. sintering temperature.

4.3.1.3 Microhardness testing

As shown in Table 4-2 and Figure 4-3, the hardness was the biggest at 700 ºC and then decreased at 750 ºC and 800 ºC. The decrease in microhardness was attributed to the change of microstructure that grain size became bigger [52]. However, there was an increase of hardness when the sintering temperature increased to 850 ºC, which could be attributed to the enhancement of connection among grains having more effects than the increasement of pore and void. Nevertheless, the density decreased to the minimum at 900 ºC. It could be found that the hardness of copper decreased as a whole with the increase of sintering temperature when the grain size and percentage of void and porosity increased that made the deformation easier. In addition, the error bar showed there were good counting statistics in 750 ºC, meaning the homogeneous microstructure of the sintered samples of as-received copper obtained.

Table 4-2 Hardness of samples made of the as-received copper powder.

Temperature (ºC)	Vickers hardness (HV)
700	61.92
750	54.2
800	53.02
850	56.89
900	52.85

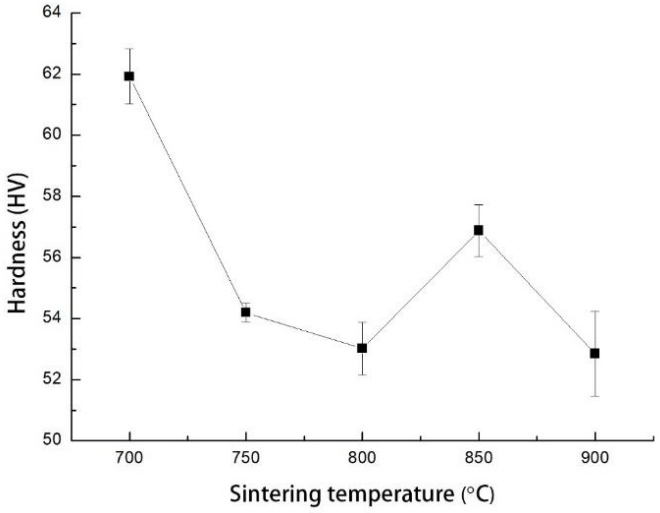

Figure 4-3 Vickers micro-hardness of as-received copper powder compacted in 850

MPa vs. sintering temperature.

4.3.2 Cu-SiC-GNP

4.3.2.1 Optical images

As displayed in Figure 4-4, the grain sizes of specimens were irregular. The light area was copper and the dark areas were Cu particles with dispersed SiC nanoparticles and GNP. It was displayed in Figures 4-4 (a) and 4-4 (b) that most particles were scattered on the surface of samples, which means that the sintering process had not finished completely. When the sintering temperature increased to 800 ºC, the aforementioned phenomenon almost disappeared and inhomogeneous grains were found due to an inadequate ball milling time. At the same time, it could be found in Figure 4-4 (c), 4-4 (d) and 4-4 (e) that more bigger-size grains were taking up a larger proportion. Furthermore, the ratio of grain boundary decreased with more grains joining together.

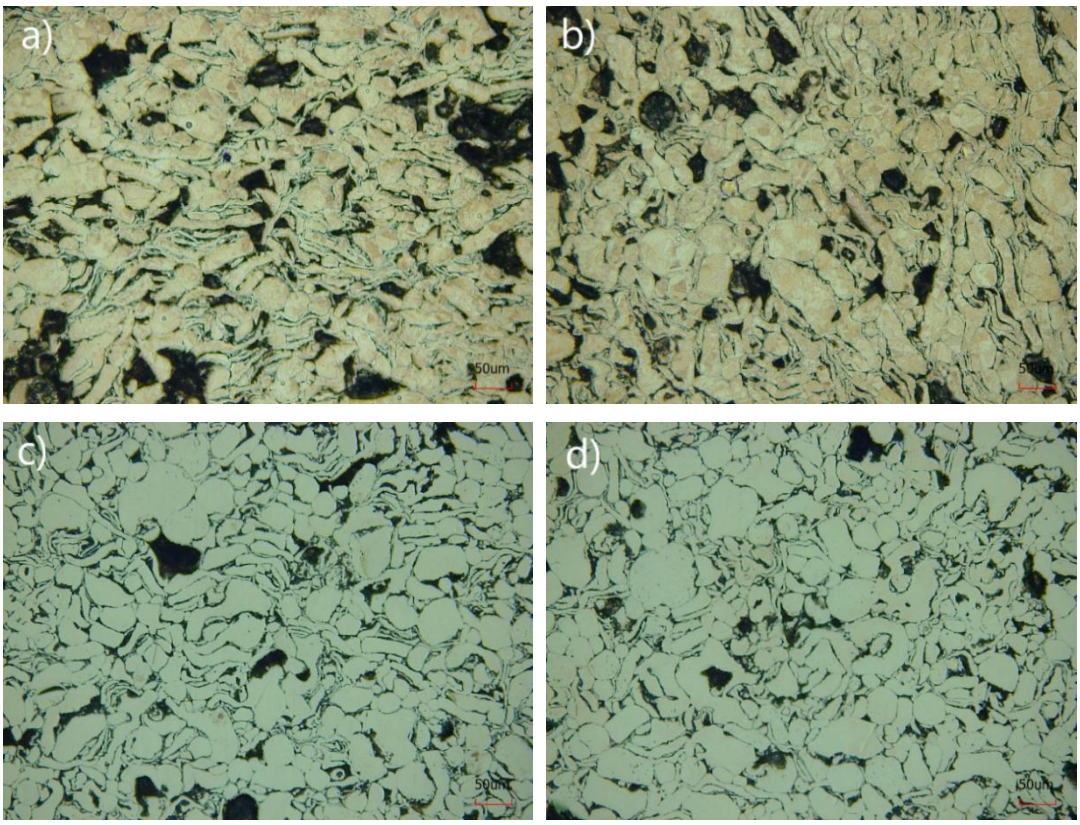

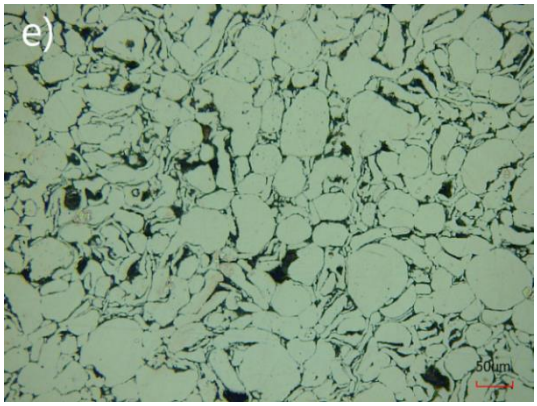

Figure 4-4 Optical micrographs of Cu-SiC-GNP composite sintered at (a) 700 ºC, (b) 750 ºC, (c) 800 ºC, (d) 850 ºC and (e) 900 ºC.

4.3.2.2 Density measurement

It was indicated in Table 4-3 and Figure 4-5 that the density of specimens increased to its maximum when the sintering temperature rose from 700 to 750 ºC, attributed to the enhanced connectivity of grains and less porosity. Then it began to decrease when the sintering temperature increased to 900 ºC due to the increase of large pore and void. The error of density showed that counting statistics at 850 and 900 ºC were a little poorer than that in other temperatures in the density measurement, meaning an inhomogeneous microstructure [127].

Table 4-3 Density of samples made of the Cu-SiC-GNP powder.

Sintering temperatures (ºC)	density (g/cm^3)	Relative density (%)	Porosity (%)
700	7.82	90.3%	9.7%
750	7.85	90.6%	9.4%
800	7.84	90.6%	9.4%
850	7.69	89.0%	11%
900	7.51	85.4%	14.6%

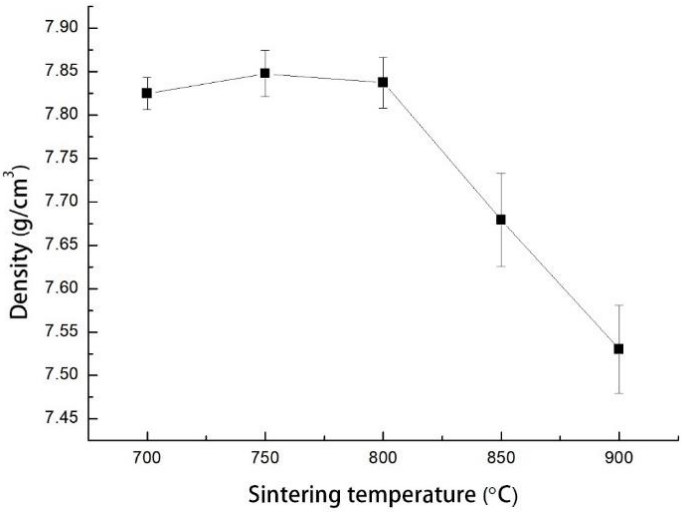

Figure 4-5 Density Cu-SiC-GNP (compacted in 850 MPa) vs. sintering temperature.

4.3.2.3 Microhardness testing

It was illustrated in Table 4-4 and Figure 4-6 that there was a slight increase for the hardness of specimens when the sintering temperature increased from 700 to 750 ºC. However, the decrease trend occurred when the sintering temperature increased from 750 to 900 ºC. It could be found that the hardness of Cu-SiC-GNP decreased as a whole with the increase of sintering temperature when the size and percentage of void and porosity increased that made the deformation easier. Furthermore, the small error showed there were good counting statistics, meaning the homogeneous microstructure of the sintered samples of Cu-SiC-GNP milled for 2 h obtained.

Table 4-4 Hardness of samples made of the Cu-SiC-GNP powder.

Sintering temperatures (ºC)	Vickers hardness (HV)
700	39.41
750	39.51
800	36.66
850	35.94
900	33.30

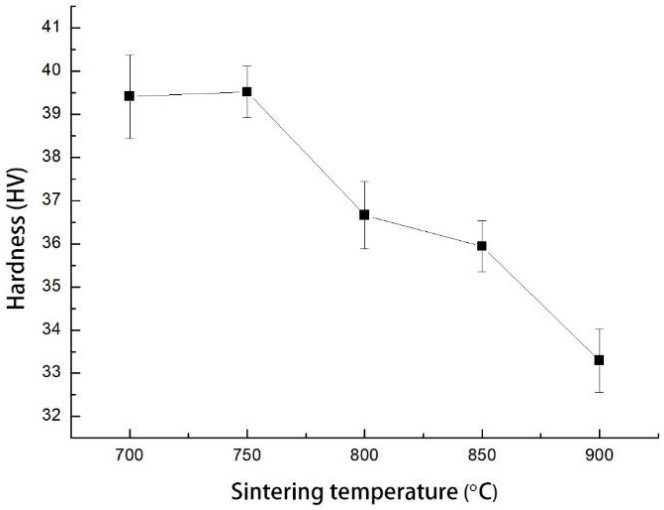

Figure 4-6 Vickers microhardness of Cu-SiC-GNP composite (compacted for 850 MPa) vs. sintering temperature.

4.4 Summary

1. For the pure copper, there were more grains joining together and more larger voids with the increase of sintering temperature. On the other hand, the sintering of Cu-SiC-GNP was not completed for 2 h at 700 and 750 ºC.

2. The highest relative density of pure copper was 95.2 % calculated from samples sintered at 800 ºC. For specimens made of Cu-SiC-GNP, the biggest relative density was 90.6% at 750 and 800 ºC.

3. The trend for hardness (against sintering temperature) of pure copper was curved and the biggest hardness of pure copper was 61.92 HV measured form specimens sintered at 700 ºC. In the term of Cu-SiC-GNP, the highest hardness was 39.51 HV observed from samples sintered at 750 ºC.

Chapter 5 Effect of milling time

5.1 Introduction

In this study, pure copper and Cu-SiC composites are fabricated as a contrast to Cu-SiC-GNP composite. Both powders and sintered specimens are investigated from the XRD patterns, SEM images, optical images, density, hardness and compressive tests.

5.2 Experimental procedure

The composites fabricated in this chapter were Cu, Cu-4vol.% SiC and Cu-4vol.% SiC-1vol.% GNP sintered at 800 ºC. Additionally, the variations with the increase of ball milling time were investigated, which focused on the morphology and chemical composites of powder samples as well as the morphology, density, microhardness and compressive strength of sintered samples. The ball milling time was mainly chosen from 0 to 8 h. Furthermore, three samples were made for each group to keep the accuracy.

5.3 Results and discussion

5.3.1 Powder analysis

5.3.1.1 SEM

1. Cu

As shown in Figures 5-1 (a) - 5-1 (e), the powder morphology of pure copper was observed at different ball milling times. Figure 5-1 (a) shows the as-received copper powder was spherical. After a 2 h ball milling, most particles were flattened due to the forces exerted from milling balls. At the same time, a slight portion of copper particles were still near-spherical, attributed to the inadequate ball milling. It could be seen that a small fraction of bigger flakes occurred due to cold welding. Therefore, the plastic

deformation took the domination during ball milling from 0 to 2 h. With a further ball milling up to 4 h, a larger proportion of flakes were formed due to cold welding. Meanwhile, a certain fraction of fragment occurred because of the increased effect of fracturing, as seen in Figure 5-1 (c). The cold welding continued to be dominant until the ball milling of 6 h, and lot of bigger flakes could be seen. However, fracturing turned predominant again with an increase of ball milling to 8 h, which was attributed to the brittleness caused by the work hardening. Therefore, a lot of flakes were broken, which were observed in Figure 5-1 (e).

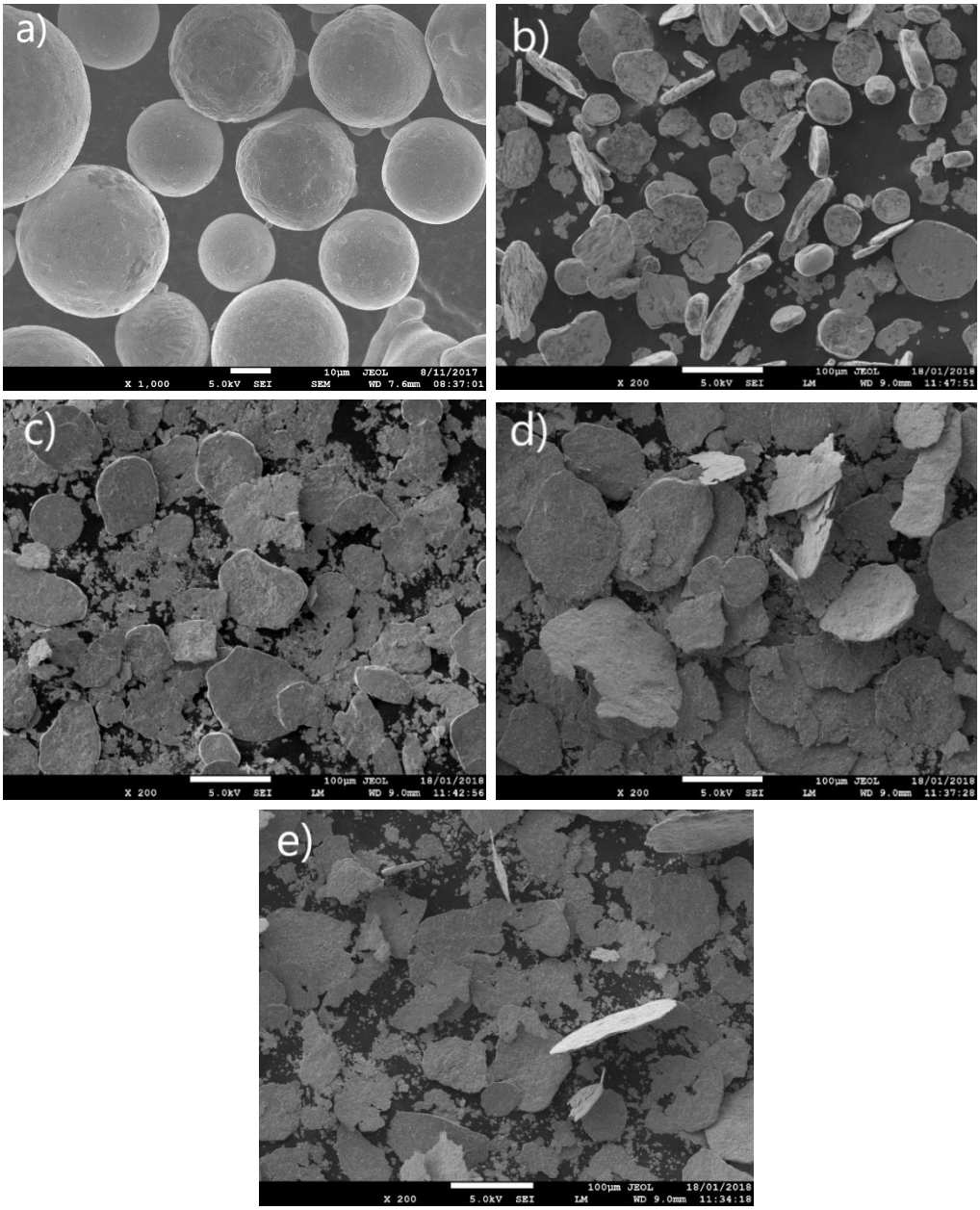

Figure 5-1 SEM micrographs of (a) as-received pure Cu powders and (b) 2 h, (c) 4 h,

(d) 6 h and (e) 8 h pure Cu powders milled.

2. Cu-SiC

As displayed in Figures 5-2 (a) - 5-2 (e), the powder morphology of Cu-SiC was observed at different ball milling times. Figure 5-2 (a) shows that most particles were flattened due to the forces exerted from milling balls after a 2 h milling. At the same time, a slight portion of particles were still near-spherical, attributed to the inadequate ball milling. It could be seen that a small fraction of bigger flakes took shape due to cold welding. Therefore, the plastic deformation took the domination during ball milling from 0 to 2 h. With the increase of time to 4 h, a bigger fraction of larger flakes took shape due to cold welding, as seen in Figure 5-2 (b). When the ball milling was prolonged to 6 h (Figure 5-2 (c)), the flakes became oval and the size of flakes was uniform due to fracturing and work hardening. The size of flakes became more uniform with the increase of ball milling to 8 h (Figure 5-2 (d)). Furthermore, the size of flakes became a bit smaller and homogenous as well until the ball milling of 20 h (Figure 5-2 (e)). Therefore, it might be predictable that the fracturing would take a significant role in the next ball milling until an equilibrium between the fracturing and the cold welding [128, 129].

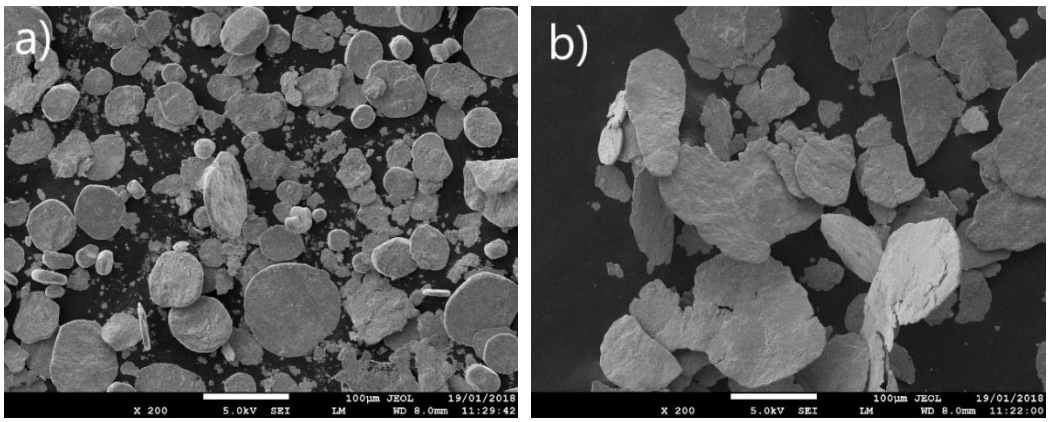

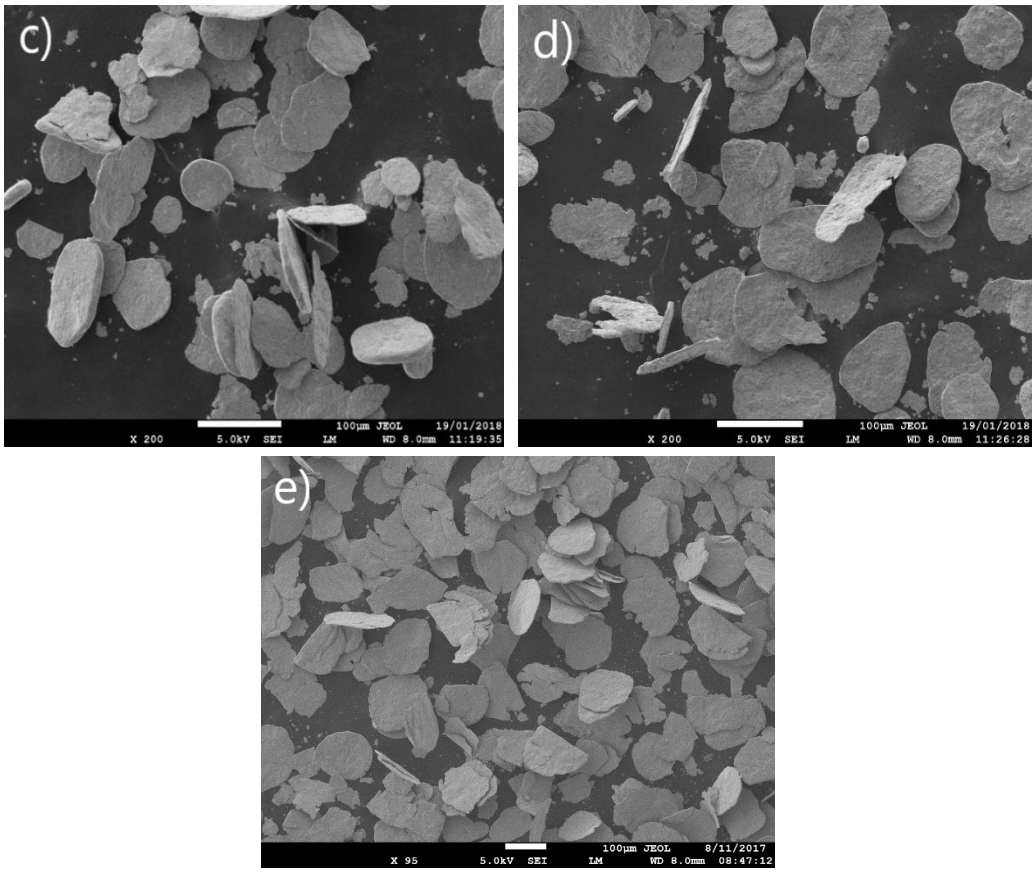

Figure 5-2 SEM micrographs of and (a) 2 h, (b) 4 h, (c) 6 h, (d) 8 h and (e) 20 h Cu-SiC powders milled.

3. Cu-SiC-GNP

As indicated in Figures 5-3 (a) - 5-3 (d), the powder morphology of Cu-SiC-GNP was observed at different ball milling time. Figure 5-3 (a) shows that most particles were milled into fragments due to the forces exerted from milling balls after a 2 h ball milling. At the same time, a little portion of particles were still near-spherical, attributed to the inadequate ball milling. It could be seen that a small fraction of bigger flakes took shape due to cold welding. Therefore, the fracturing took the domination during ball milling from 0 to 2 h. With a further ball milling to 4 h, lots of flakes in inhomogeneous size were produced attributed to cold welding (Figure 5-3 (b)). With the increase of ball milling, flakes became larger and more homogeneous and near-equiaxed because of the continuing cold welding. Similarly, the size and distribution of flakes were almost the same. Therefore, it is predicted that the ball milling will come to a stabilised situation

with further ball milling [129].

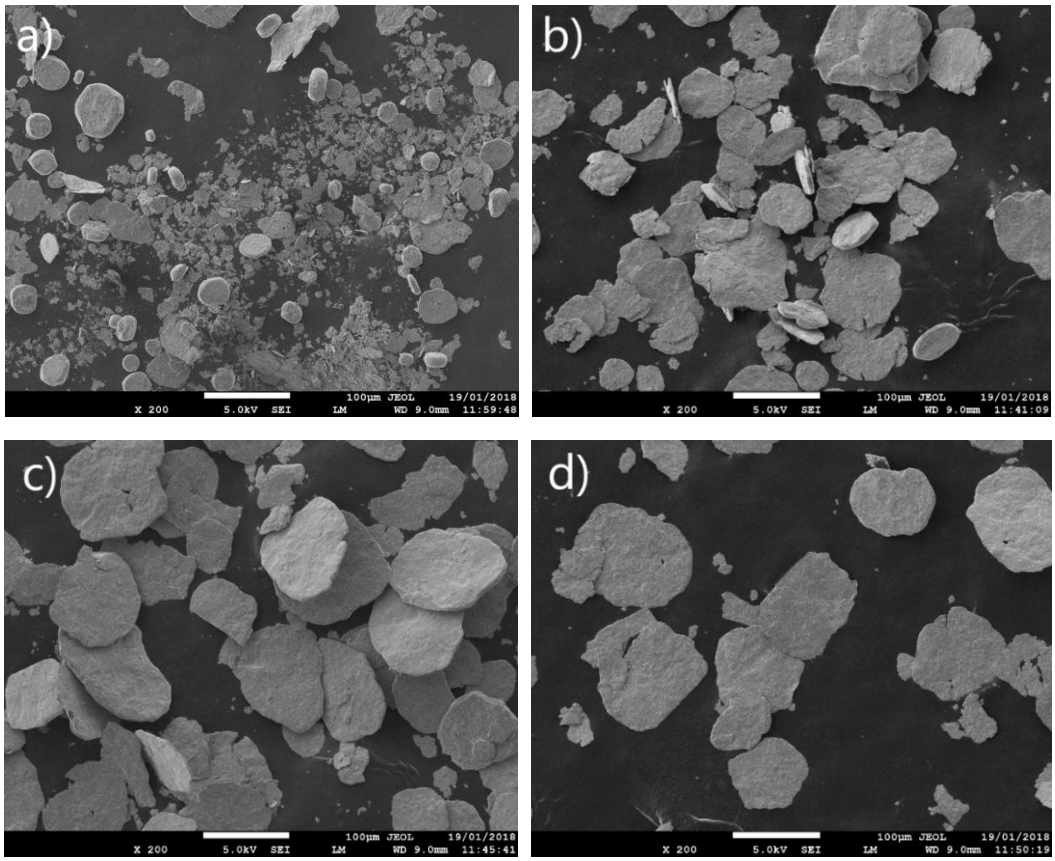

Figure 5-3 SEM micrographs of (a) 2 h, (b) 4 h, (c) 6 h and (d) 8 h Cu-SiC-GNP powders milled.

5.3.1.2 XRD analysis

1. Cu

The XRD patterns of Cu milled for different times are shown in Figure 5-4. It could be found that indices of crystal faces, which were for different XRD patterns of Cu powders milled for 2, 4, 6 and 8 h, were the same as the as-received copper powder. Furthermore, there were not changes in the geometry or other diffraction peaks, meaning no undesirable reactions like oxidation or a slight volume of unexpected reaction production in the ball milling process [62]. At the same time, peaks at (2 0 0) increased bigger relatively in the ball milling. The peak width and intensities changed

irregularly.

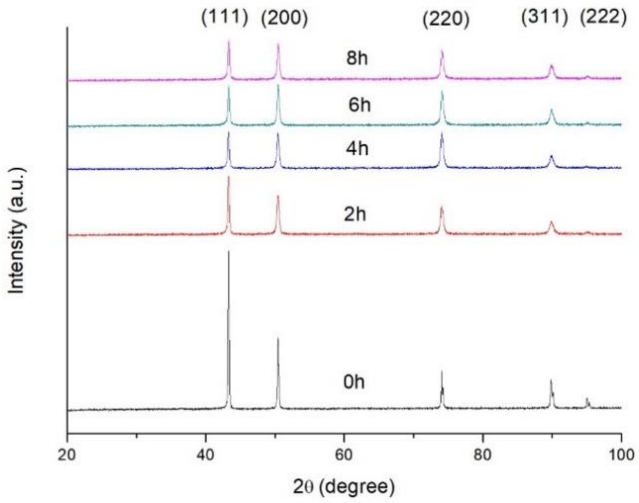

Figure 5-4 XRD patterns of Cu milled for 0, 2, 4, 6 and 8 h.

As mentioned before, the crystallite size could be estimated from the following W-H equation (Equation (5-1)) according to the linear fit of $4\sin\theta_{hkl}$ and $\cos\theta_{hkl}$ by the software Origin. In the construction of the liner plot (Figure 5-5), the five peaks (1 1 1), (2 0 0), (2 2 0), (3 1 1) and (2 2 2) were used. β_{hkl} and θ_{hkl} could be found from the XRD after the processing of the software Jade.

$$\beta_{hkl}\cos\theta_{hkl} = \left(\frac{K\lambda}{t}\right) + 4\varepsilon\sin\theta_{hkl} \tag{5-1}$$

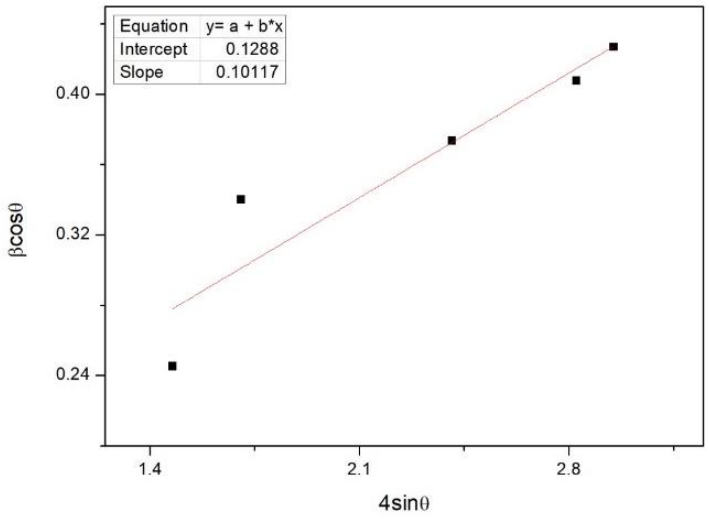

Figure 5-5 W-H plots for Cu powder milled for 2 h.

The trend of the grain size of the milled Cu powder for different ball milling times is displayed in Figure 5-6. It could be seen that after the 2 h ball milling, the grain size rose to around 1.1 nm, attributed to the cold welding. Then it decreased to the minimum value around 0.5 nm in the next 4 h ball milling. Nevertheless, it increased to 0.7 nm when the ball milling time reached 8 h. Therefore, the trend corresponds with the irregular change of XRD patterns.

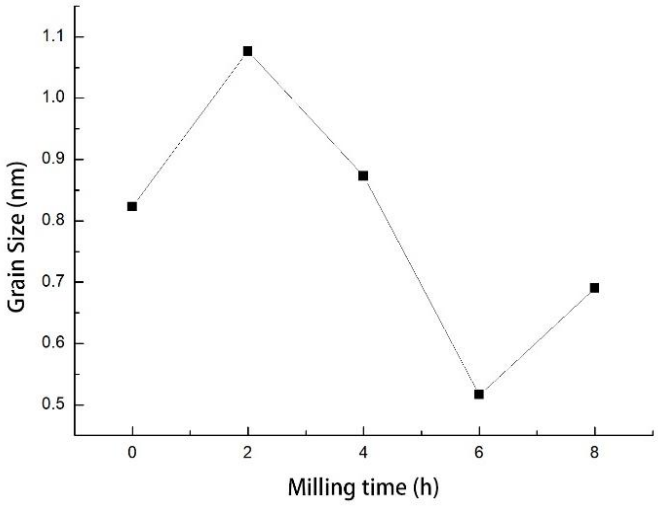

Figure 5-6 Grain size vs. milling time for copper powder.

2. Cu-SiC

The XRD patterns of Cu-4 vol% SiC milled for different times are indicated in Figure 5-7. It could be found that indices of crystal faces, which were for different XRD patterns of Cu powders milled for 2, 4, 6 and 8 h, were the same as the as-received copper powder. Furthermore, there were not changes in the geometry or other diffraction peaks, meaning no undesirable reactions like oxidation or undeted volume of unexpected reaction production in the ball milling process [62]. At the same time, peaks at (2 0 0) increased bigger relatively in the ball milling. The peak width and peak intensities changed irregularly.

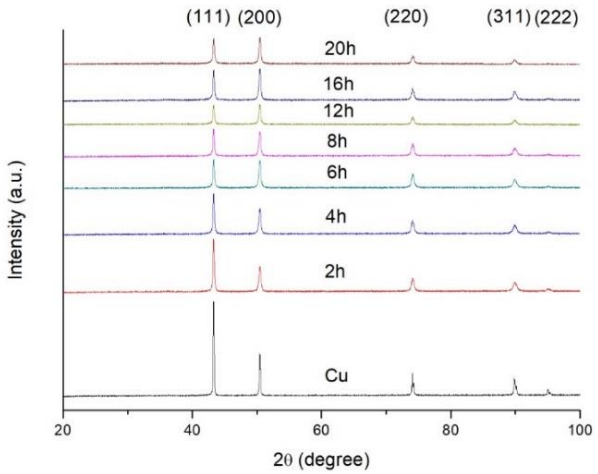

Figure 5-7 XRD patterns of the as-received pure copper powder and Cu-SiC powder milled for 2, 4, 6, 8, 12, 16 and 20 h.

As shown in Figure 5-8, the trend of changes for the grain size of the milled Cu-SiC powder for different ball milling times was curved. It could be seen that after the 2 h ball milling, the grain size was around 0.93 nm. Then it slightly decreased to 0.92 nm after 4 h ball milling, and then it declined sharply to the minimum 0.65 nm until the powders were milled for 6 h, and then it increased to 0.95 nm when the ball milling time was prolonged to 8 h, followed by a decrease again until it was milled for 20 h. It reduced to 0.77 nm quickly from 10 to 12 h. In the next ball milling, it decreased slowly to 0.65 nm where the ball milling came to a steady-state equilibrium, where the cold welding and fracturing of powders were in balance [130]. Compared to the pure Cu powder, Cu-SiC is expected to become smaller, attributed to the latter undergoing severer plastic deformation in the presence of SiC nanoparticles and enhanced dislocation density.

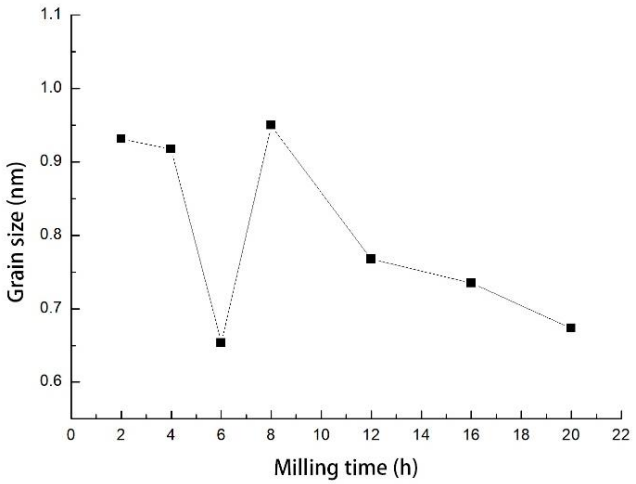

Figure 5-8 Grain size vs. milling time for Cu-SiC powder.

3. Cu-SiC-GNP

The XRD patterns of Cu-4 vol% SiC-1 vol% GNP milled for different times are indicated in Figure 5-9. It could be found that indices of crystal faces, which were for different XRD patterns of Cu powders milled for 2, 4, 6 and 8 h, were same as the as-received copper powder, attributed to the low ratio of SiC and GNP in the mixed powders. Furthermore, there were not changes in the geometry or other diffraction peaks, meaning no undesirable reactions like oxidation or undetected volume of unexpected reaction production in the ball milling process [62]. At the same time, peaks at (2 0 0) increased bigger relatively in the ball milling, and the peak width and intensities changed irregularly.

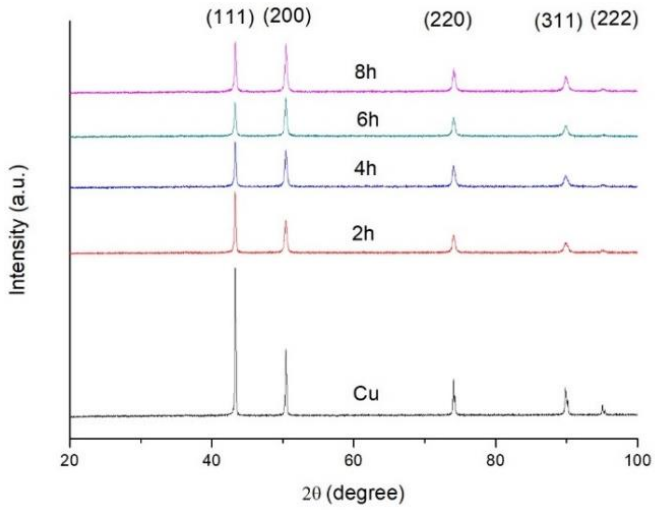

Figure 5-9 XRD patterns of the as-received pure copper powder and Cu-SiC-GNP milled for 2, 4, 6 and 8 h.

As displayed in Figure 5-10, the trend of changes for the grain size of the milled Cu-SiC-GNP powder for different ball milling times was curved. It could be seen that after 2 h ball milling, the grain size was around 1.05 nm. Then it reduced sharply to 0.72 nm when the ball milling was prolonged to 4 h, and then it increased a bit to 0.85 nm after 6 h ball milling. However, it decreased to 0.62 nm again after another 2 h ball milling. Therefore the trend corresponds with the irregular change of XRD patterns. Compared to the pure Cu powder, Cu-SiC is expected to become smaller, attributed to the latter undergoing severer plastic deformation in the presence of SiC nanoparticles and enhanced dislocation density.

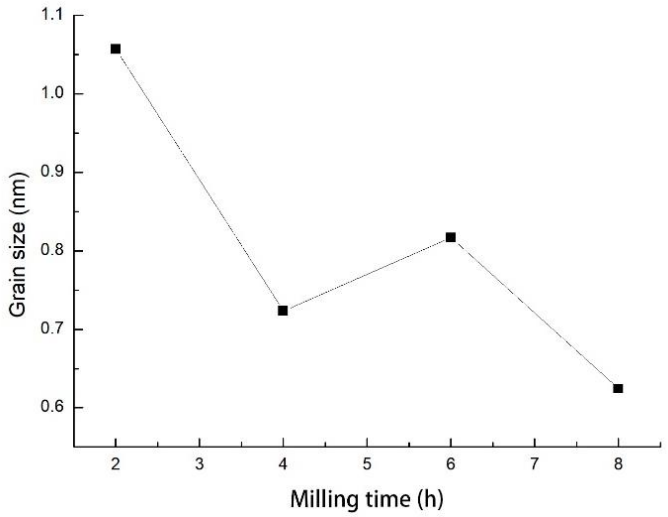

Figure 5-10 Grain size vs. milling time for Cu-SiC-GNP powder.

5.3.2 Analysis of sintered composites

5.3.2.1 Optical images

1. Cu

The optical micrographs of sintered samples for pure copper are shown in Figure 5-11. The morphology of Cu is consistent with the optical microscopy (OM) images of Cabeza et al. [55]. As mentioned in the analysis of powder, with the increase of ball milling time, a bigger ratio of flake particles occurs from 2 to 8 h. The size and shapes of flakes have a tendency to be uniform. The dark area is CuO due to a slight volume of oxidation during sintering.

As displayed in Figure 5-11 (a), particles of irregular round shapes and different sizes were observed together after sintering, consistent with the powder morphology of Cu milled for 2 h. After a ball milling of 4 h, a little ratio of flattened particles that stacked together and particles with bigger surface could be found in Figure 5-11 (b). The distribution of particles in the cross section could be attributed to the cold pressing. Under the forces from the die, particles are pushed mutually. As a consequence, flattened particles would form vertically under the pushing from other particles in

vicinity. Therefore, an increasing percentage of flakes particles stacking together appeared when the ball milling was prolonged to 6 and 8 h, as observed in Figures 5-11 (c) and 5-11 (d).

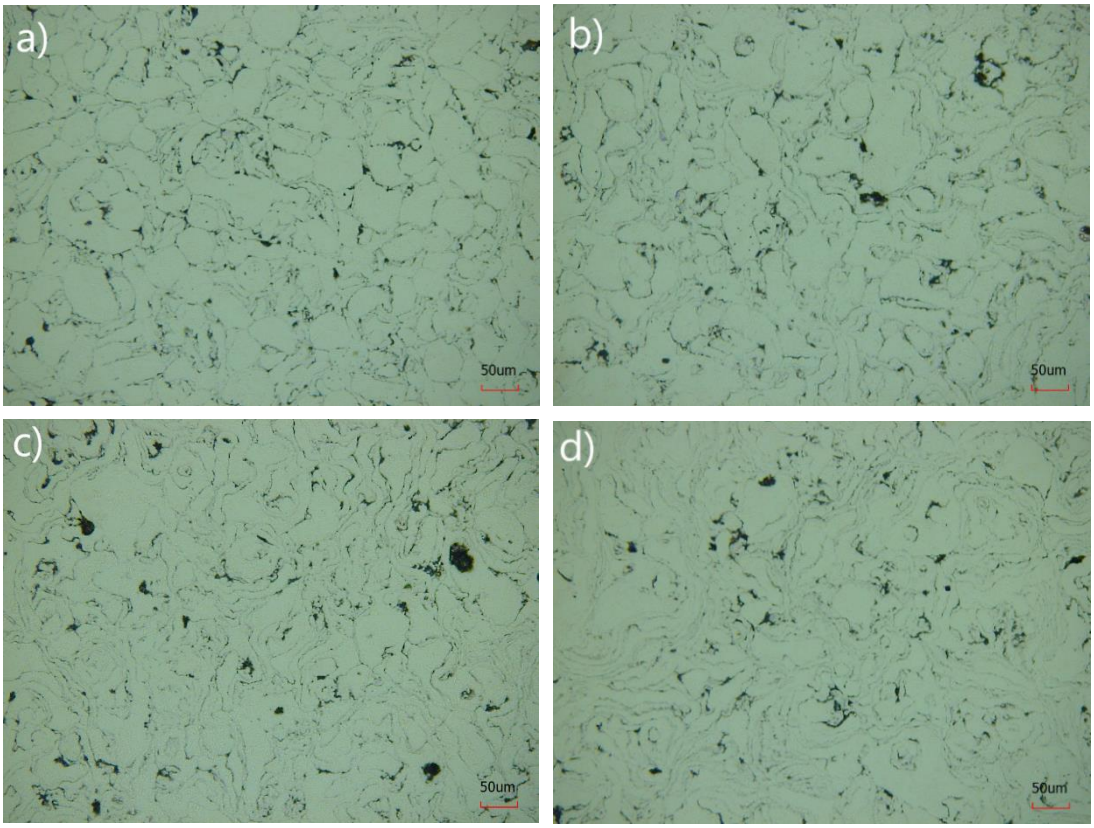

Figure 5-11 Optical micrographs of Cu milled for (a) 2 h, (b) 4 h, (c) 6 h and (d) 8 h.

2. Cu-SiC

The optical micrographs of bulk samples for Cu-SiC composites are displayed in Figure 5-12, corresponding with the aforementioned analysis of Cu-SiC powders. As indicated in Figure 5-12, the morphology for Cu-SiC had a similar tendency to change with the increase of ball milling time. The morphology of Cu-SiC is consistent with the OM images of Cabeza et al. [55]. The dark areas are the Cu particles with dispersed SiC nanoparticles.

As shown in Figure 5-12(a), particles of irregular round shapes and different sizes were

observed together after sintering, consistent with the powder morphology of Cu-SiC milled for 2 h. After a ball milling of 4 h, flattened particles that stacked together and particles with bigger surface could be found in Figure 5-12 (b). The distribution of particles in the cross section could be attributed to the cold pressing. Under the forces from the walls of punches, particles are pushed mutually. As a consequence, flattened particles would form vertically under the pushing from other particles in vicinity. Therefore, an increasing percentage of flakes particles stacking together appeared when the ball milling was prolonged to 6 and 8 h, as observed in Figures 5-12 (c) and 5-12 (d).

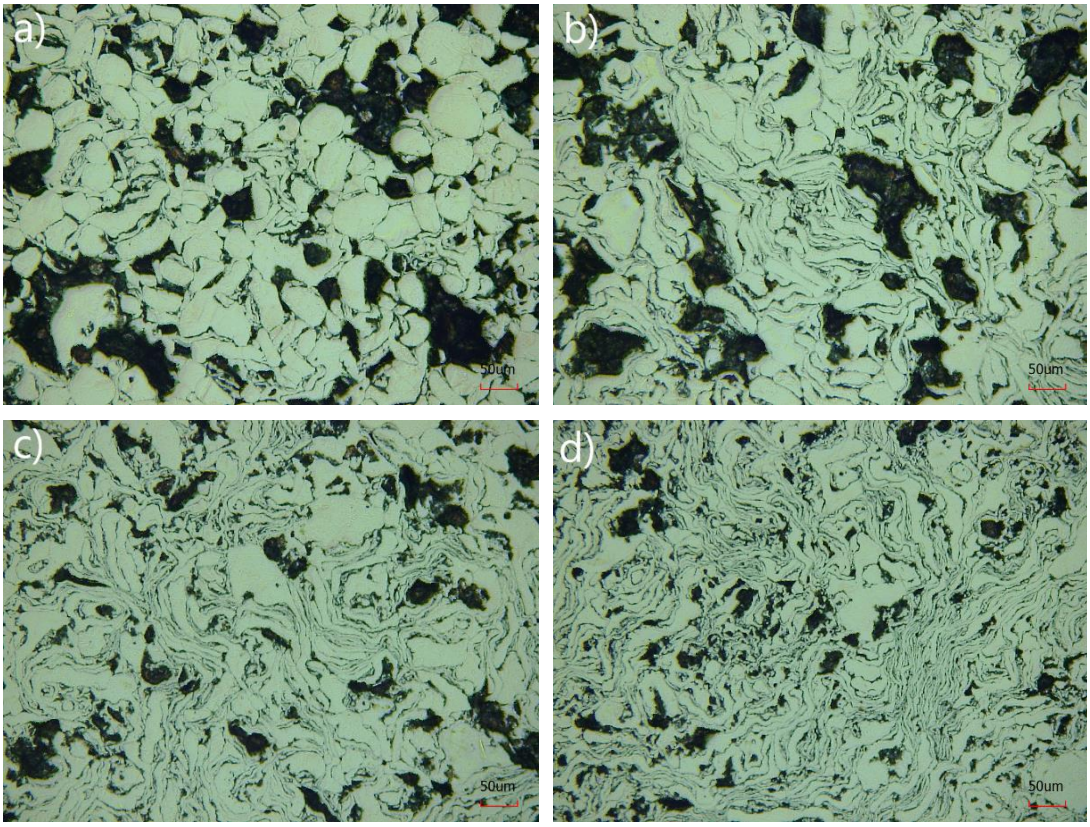

Figure 5-12 Optical micrographs of Cu-SiC milled for (a) 2 h, (b) 4 h, (c) 6 h and (d) 8 h.

3. Cu-SiC-GNP

The optical micrographs of bulk samples for Cu-SiC-GNP composites are displayed in Figure 5-13, corresponding with the aforementioned analysis of Cu-SiC-GNP powders.

As displayed in Figure 5-13, the morphology for Cu-SiC-GNP had a similar tendency to change with the increase of ball milling time. The morphology of Cu-SiC-GNP is consistent with the OM images of Cabeza et al. [55]. The dark areas are Cu particles with dispersed SiC nanoparticles and GNP.

As shown in Figure 5-13 (a), particles of irregular round shapes and different sizes were observed together after sintering, consistent with the powder morphology of Cu-SiC-GNP milled for 2 h. After a ball milling of 4 h, a slight ratio of flattened particles that stacked together and particles with bigger surface could be found in Figure 5-13 (b). The distribution of particles in the cross section could be attributed to the cold pressing. Under the forces from the walls of punches, particles are pushed mutually. As a consequence, flattened particles would form vertically under the pushing from other particles in vicinity. Therefore, an increasing percentage of flakes particles stacking together appeared when the ball milling was prolonged to 6 h and 8 h, as observed in Figures 5-13 (c) and 5-13 (d).

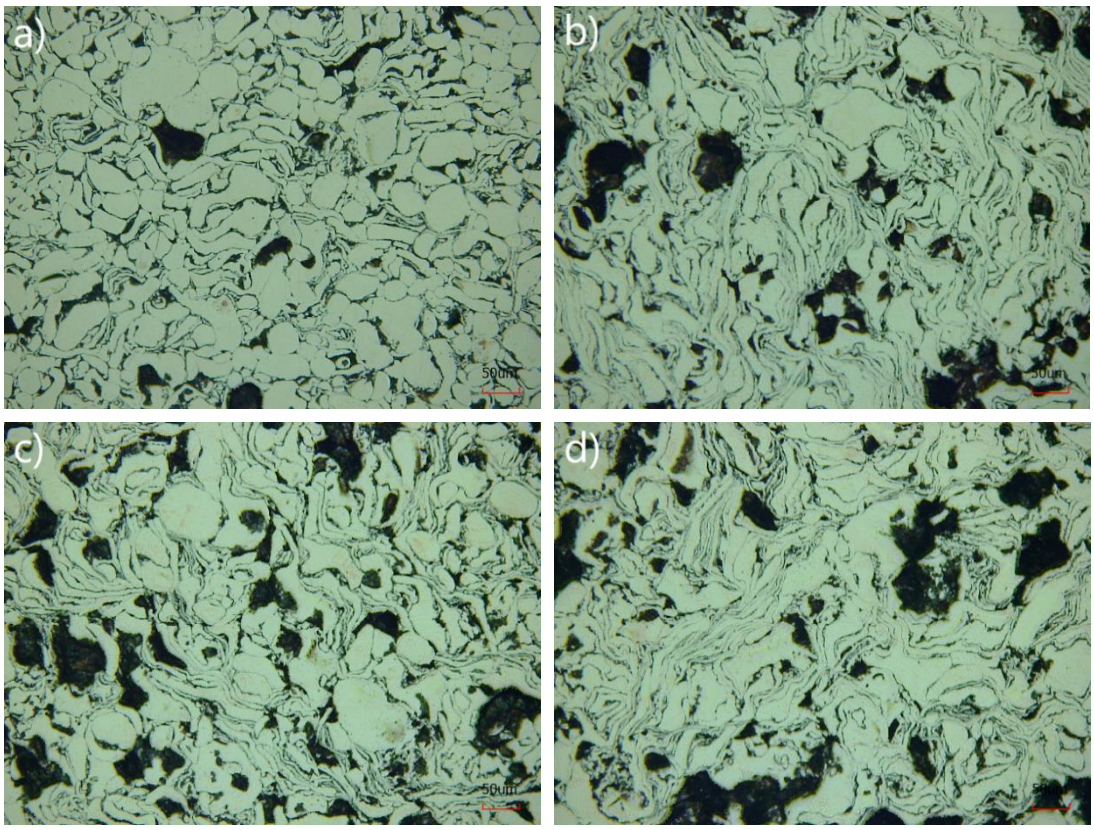

Figure 5-13 Optical micrographs of Cu-SiC-GNP milled for (a) 2 h, (b) 4 h, (c) 6 h

and (d) 8 h.

5.3.2.2 Density measurement

1. Cu

As indicated in Table 5-1 and Figure 5-14, the density decreased from 8.1 g/cm^3 at 2 h to 7.94 g/cm^3 at 6 h. Nevertheless, it increased to 8.02 g/cm^3 when the ball milling was prolonged to 8 h. It could be seen in Table 5-1 that the biggest relative density was 90.4 %, where the porosity reached the minimum 9.6 %. Therefore the density intended to decline in general with the increase of ball milling time within 8 h. The trend is consistent with the research of Fogagnolo et al. [56]. Furthermore, the error bar of density showed a good counting statistics in the density measurement [127].

To explain the result, the hardening effect could be taken into account on the one hand. According the investigation of Gan & Gu [57], the green density of compacts declines due to the work hardening, which increased its hardness of the sintering. On the other hand, the morphology of particles may have its influence on the density. In this case, the laminar morphology is taking an increasing proportion with the ball milling time. In the process of compacting, the irregular morphology might cause the shear deformation that brings about the cold welding under the compressive stress, making it hard for the compacting and the sintering afterwards.

Table 5-1 Density of samples made of the milled copper powder.

Ball milling time (h)	Theoretical density (g/cm^3)	Relative density (%)	Porosity (%)
2	8.1	90.4	9.6
4	8.05	89.84	10.16
6	7.94	88.62	11.28
8	8.02	89.61	10.39

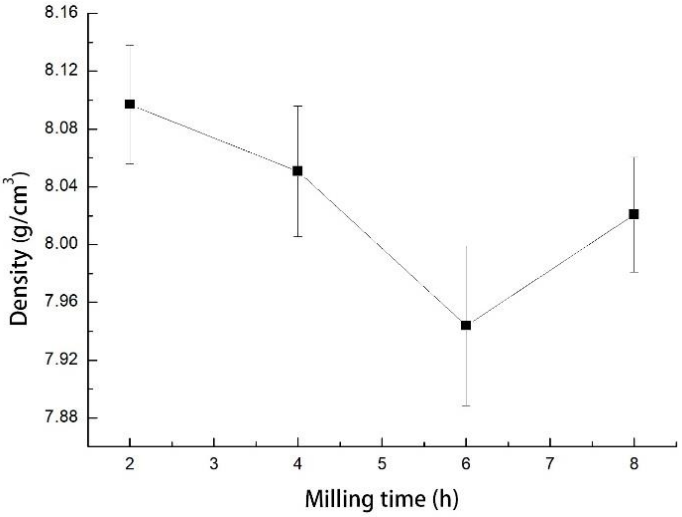

Figure 5-14 Density of milled copper vs. milling time of 2, 4, 6 and 8 h.

2. Cu-SiC

As shown in Table 5-2 and Figure 5-15, the density of Cu-SiC continued to decreased from 7.65 g/cm^3 at 2 h to 7.02 g/cm^3 at 8 h. The biggest relative density in Table 5-2 for Cu-SiC was 87.63 %, with the smallest porosity of 12.37 %. The decreasing trend is in consistence with the research of Fogagnolo et al. [56]. As mentioned before, the work hardening and the morphology of particles might contributed to the decrease of density with the increase of ball milling [56, 57]. Additionally, the error bar of density showed good counting statistics in the density measurement [127].

Table 5-2 Density of samples made of the Cu-SiC powder.

Ball milling time (h)	Theoretical density (g/cm^3)	Relative density (%)	Porosity (%)
2	7.65	87.63	12.37
4	7.56	86.6	13.4
6	7.28	83.4	16.6
8	7.02	80.42	19.58

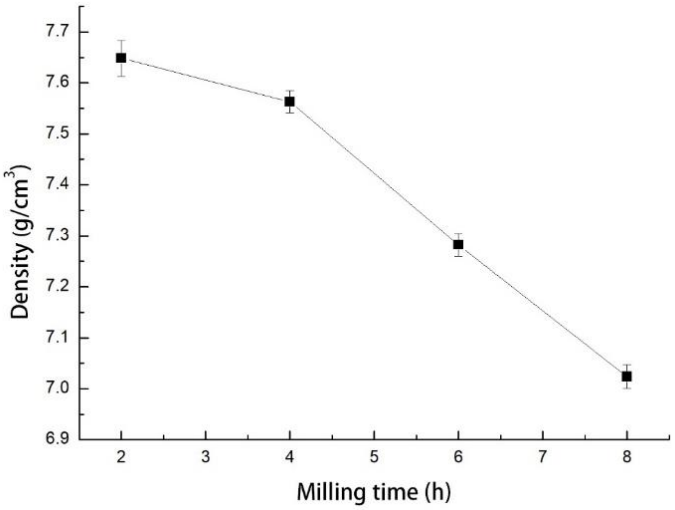

Figure 5-15 Density Cu-SiC composite vs. milling time of 2, 4, 6 and 8 h.

3. Cu-SiC-GNP

As displayed in Table 5-3 and Figure 5-16, the density of Cu-SiC-GNP continued to decrease from 7.84 g/cm^3 at 2 h to 7.38 g/cm^3 at 4 h. However, there was a bit of increase in density at 6 h. It decreased to 7.09 g/cm^3 at 8 h. The biggest relative density in Table 5-3 for Cu-SiC-GNP was 90.51 %, with the smallest porosity of 9.49 %. Generally, the trend was in decrease, consistent with the research of Fogagnolo et al. [22]. As mentioned before, the work hardening and the morphology of particles might contribute to the decrease of density with the increase of ball milling time [56, 57]. In addition, the error bar of density showed good counting statistics in the density measurement [127].

Table 5-3 Density of samples made of the Cu-SiC-GNP powder.

Ball milling time (h)	Theoretical density (g/cm^3)	Relative density (%)	Porosity (%)
2	7.84	90.51	9.49
4	7.38	85.19	14.81
6	7.43	85.77	14.23
8	7.09	81.85	18.15

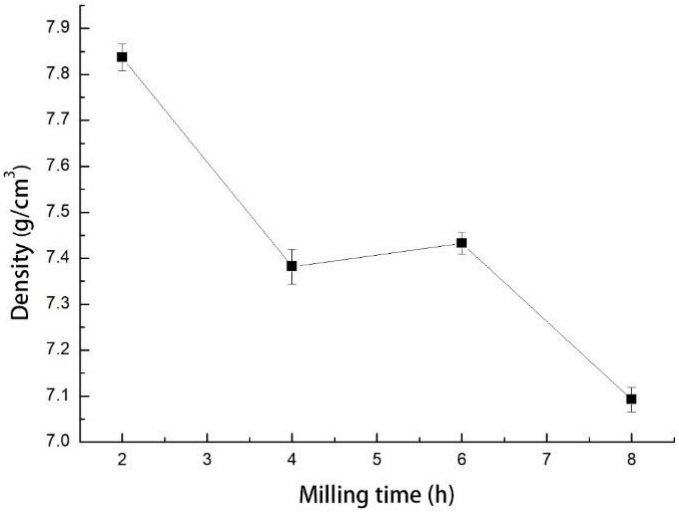

Figure 5-16 Density of Cu-SiC-GNP vs. milling time of 2, 4, 6 and 8 h.

5.3.2.3 Microhardness testing

1. Cu

The trend for the hardness of Cu with the ball milling time is displayed in Figure 5-17. The hardness started from 41.39 HV at 2 h to 40 HV at 4 h at first. Then it increased to 43.65 HV that was the maximum of the hardness at 6 h. Then there was another decrease after 6 h, where the hardness was 43.04 HV at 8 h. In general, the hardness was improved by ball milling. The behavior could be attributed to the changes of microstructure and morphology under the ball milling, which caused the work hardening of powders [131]. Moreover, the small error bar showed there were good counting statistics, meaning the homogeneous microstructure of the sintered samples of milled copper.

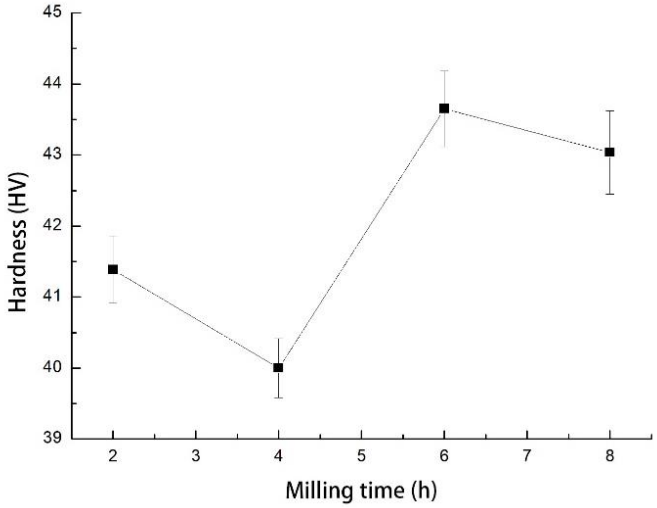

Figure 5-17 Hardness of copper vs. milling time of 2, 4, 6 and 8 h.

2. Cu-SiC

The trend for the hardness of Cu-SiC with the ball milling time is displayed in Figure 5-18. The hardness started from 41.06 HV at 2 h to 39.08 HV at 4 h at first. Then it increased to 51.01 HV that was the maximum of the hardness at 6 h. Then there was another decrease after 6 h, where the hardness was 48.42 HV at 8 h. In general, the hardness was improved by ball milling.

The increase in hardness of Cu-SiC with the ball milling time might ascribed to the work hardening and the refinement of particles [55, 131]. As mentioned before, the work hardening was attributed to the changes of microstructure and morphology under the milling device during ball milling. Furthermore, the locally internal strain caused by the deformation would increase the density of dislocation and grain refinement, which enhance the hardness [132, 133]. In addition, the uniform dispersion of SiC nanoparticles in the Cu matrix could inhibit the grain growth, enhancing the grain refinement [134]. Furthermore, the small error bar showed there were good counting statistics, meaning the homogeneous microstructure of the sintered samples of Cu-SiC obtained.

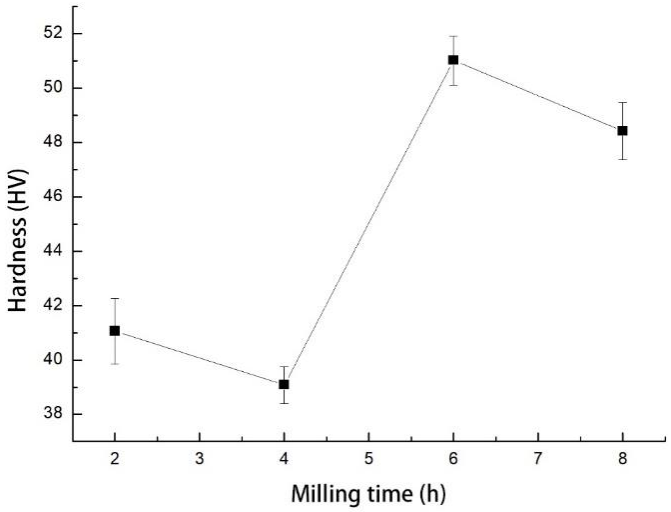

Figure 5-18 Hardness of Cu-SiC vs. milling time of 2, 4, 6 and 8 h.

3. Cu-SiC-GNP

The trend for the hardness of Cu-SiC-GNP with the ball milling time is displayed in Figure 5-19. The hardness started from 36.66 HV at 2 h to 32.63 HV at 4 h at first. Then it increased to 49.32 HV that was the maximum of the hardness at 6 h. Then there was another decrease at 6 h, where the hardness was 45.45 HV. In general, the hardness was improved by the ball milling. Moreover, the small error bar showed there were good counting statistics, meaning the homogeneous microstructure of the sintered samples of Cu-SiC-GNP. As mentioned in Cu-SiC, the increase in hardness of Cu-SiC-GNP with the ball milling time might ascribed to the work hardening and the refinement of particles [55, 131].

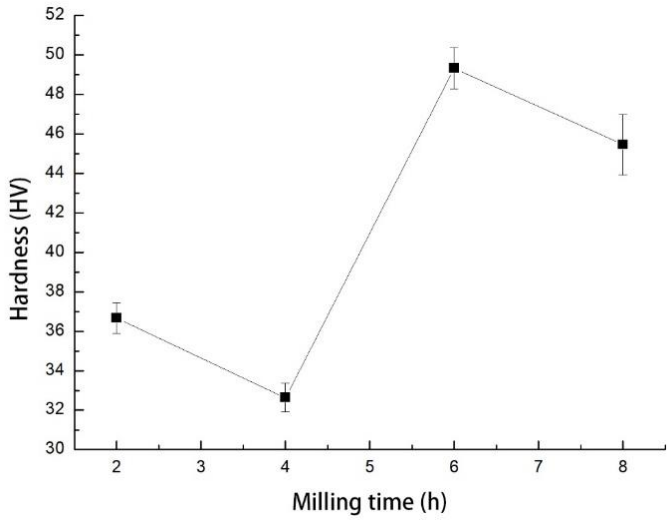

Figure 5-19 Hardness of Cu-SiC-GNP vs. milling time of 2, 4, 6 and 8 h.

5.3.2.4 Compressive testing

1. Cu

The strain-stress curve and results of compressive testing of Cu are shown in Figure 5-20 and Table 5-4. Pre-loading data produced during the non-intimate contact was eliminated [61]. It could be found that the yield strength increased with the increase of ball milling time from 0 to 8 h, and there was almost no enhancement in the maximum of compressive stress within the engineering strain of 0.4. The enhancement in the yield strength was attributed to the increments of dislocation density and particle grain refinements. Additionally, it could be observed that both the maximum of compressive stress and yield strength of Cu milled from 2 to 8 h were lower than that of the as-received Cu, ascribed to the contrast between the irregular morphology of milled copper and the homogeneously spherical morphology of as-received copper.

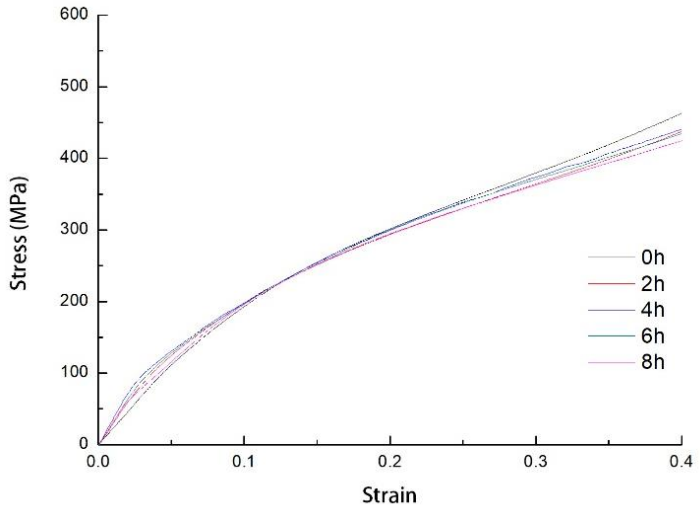

Figure 5-20 Compressive strain-stress curves of Cu milled for 0, 2, 4, 6 and 8 h.

Table 5-4 Results of compression testing of Cu.

Ball milling time (h)	Max.compressive stress (MPa)	Compressive yield point (MPa)
0	469	159.57
2	429	80.21
4	448	87.85
6	434	96.61
8	434	109.4

2. Cu-SiC

The strain-stress curve and results of compressive testing of Cu-SiC are displayed in Figure 5-21 and Table 5-5. It could be found that both the maximum of compressive stress and yield strength of Cu-SiC had a tendency to increase with the increase of ball milling time. The obvious increase could be ascribed to: grain refinement, the increase of dislocation density caused by mismatch of CTE, load transferring from the matrix to reinforcements and Orowan strengthening mechanisms as mentioned before.

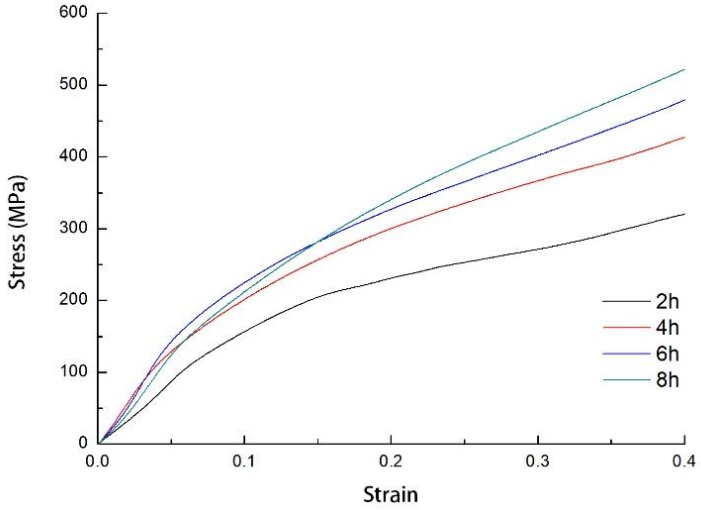

Figure 5-21 Compressive strain-stress curves of Cu-SiC milled for 2, 4, 6 and 8 h.

Table 5-5 Results of compression testing of Cu-SiC.

Ball milling time (h)	Max.compressive stress (MPa)	Compressive yield point (MPa)
2	335	138.31
4	433	114.28
6	479	218.28
8	522	275.38

3. Cu-SiC-GNP

The strain-stress curve and results of compressive testing of Cu-SiC-GNP are shown in Figure 5-22 and Table 5-6. It could be observed that the maximum of compressive stress of Cu-SiC-GNP had a tendency to decrease with the prolonged ball milling time, but the yield point of Cu-SiC-GNP changed irregularly with the increase of ball milling time. The variation of compressive properties could be attributed to irregular morphology of Cu-SiC-GNP particles and the ball milling time that was not long enough to disperse both the SiC nanoparticles and graphene nanoplates homogeneously in the Cu matrix.

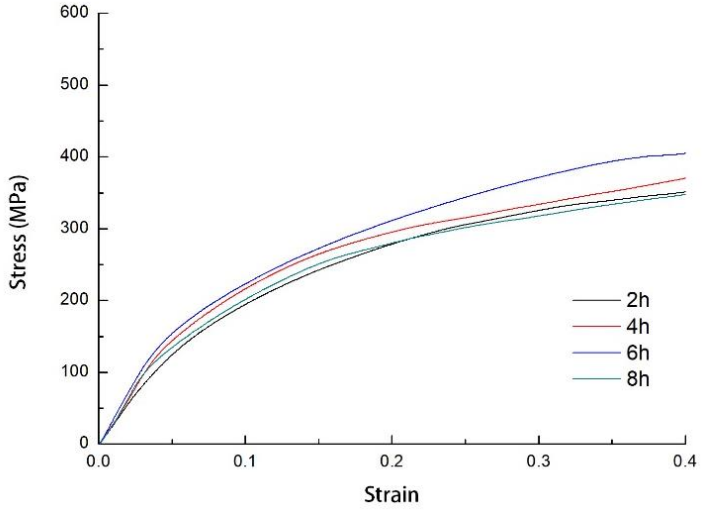

Figure 5-22 Compressive strain-stress curves of Cu-SiC-GNP milled for 2, 4, 6 and 8 h.

Table 5-6 Results of compression testing of Cu-SiC-GNP.

Ball milling time (h)	Max.compressive stress (MPa)	Compressive yield point (MPa)
2	384	118.82
4	370	149.72
6	377	114.65
8	347	126.59

5.4 Summary

In this study, the powder and sintered samples of pure copper, Cu-SiC composites and Cu-SiC-GNP are investigated through XRD, SEM, optical microscope, automatic density measuring machine and hardness testing machine. The variation in different properties of samples is summarised as follows:

(1) The evolution in morphology of Cu, Cu-SiC and Cu-SiC-GNP was similar from 0 h to 8 h. At first, most particles were flattened during plastic deformation and cold welding. Then the powders turned into flakes with similar size due to the balance between cold welding and fracturing at 8 h.

(2) There were any other diffraction peaks in the XRD patterns of Cu, Cu-SiC and

Cu-SiC-GNP except for the peaks of Cu, meaning no undesirable reactions or just a little volume of unexpected reaction happened in the ball milling process of 8 h. The trend of grain size of these three different materials was not linear during the ball milling of 8 h. However, the grain size of Cu-SiC decreased continuously when it was prolonged from 8 to 12 h.

(3) The evolution in morphology of sintered Cu, Cu-SiC and Cu-SiC-GNP was similar from 0 to 8 h. With the increase of ball milling time, the phenomenon of stacking among vertical flakes particles became more obvious due to the effect of cold pressing.

(4) The theoretical density against the ball milling time of Cu, Cu-SiC and Cu-SiC-GNP had different trends. The relative density of Cu reached the maximum of 90.4 % at 2 h and 88.62 % at 6 h. The relative density of Cu-SiC attained the maximum of 87.63 % at 2 h and 80.42 % at 8 h. The relative density of Cu-SiC-GNP attained the maximum of 90.51% at 2 h and 81.85 % at 8 h. In general, the density intended to decrease with the increase of ball milling time due to the work hardening and the laminar (or flake) shape of particles. Densities of Cu-SiC and Cu-SiC-GNP were lower than that of Cu because of lower densities of SiC and GNP.

(5) The hardness of sintered samples for Cu, Cu-SiC and Cu-SiC-GNP showed a similar trend with the increase of ball milling time. The hardness of Cu reached the maximum of 43.65 HV at 6 h and the minimum of 40.00 HV at 4 h. The hardness of Cu-SiC composite attained the maximum of 51.01 HV at 6 h and the minimum of 39.08 HV at 4 h. The hardness of Cu-SiC-GNP composite reached the maximum of 49.32 HV at 6 h and the minimum of 32.63 HV at 4 h. In general, the hardness of Cu, Cu-SiC and Cu-SiC-GNP intended to increase with the increase of ball milling time due to the work hardening and the refinement of particles. It could be seen that the biggest densites of Cu-SiC and

Cu-SiC-GNP were bigger than that of Cu. Additionally, the biggest density of Cu-SiC was bigger than that of Cu-SiC-GNP.

(6) The compressive properties of Cu, Cu-SiC and Cu-SiC-GNP had different trends with the increase of ball milling time. The yield point of Cu increased with the prolonged ball milling time and reached to 109.4 MPa at 8 h due to the increments of dislocation density and particle grain refinements. As for Cu-SiC, both the yield point and maximum of compressive stress had a tendency to increase from 2 to 8 h, and they reached the maximum of 275.38 MPa and 522 MPa respectively. The compressive yield point of Cu-SiC-GNP obtained the maximum of 149.72 MPa, and the compressive stress of Cu-SiC-GNP obtained the maximum of 384 MPa at 2 h.

Chapter 6 Conclusion and future work

6.1 Conclusions

In this study, a combination of the graphene with the traditional metal matrix composites was put forward, which was to exert the advantage of graphene and fabricate a new material that is available for some applications. In this study, planetary ball milling, cold pressing and sintering were used to fabricate the Cu-4 vol % SiC-1 vol % GNP, which provided a route for the industrial manufacturing of Cu-SiC-GNP. Basic parameters like milling balls and compaction molds worked properly in the experiment. The route functioned well in the fabrication, which was very efficient.

Different parameters were utilised to find the appropriate condition to achieve the samples with superior properties. Firstly, sintering temperature was taken as a factor to observe the change of morphology of bulk samples. The as-received Cu powder and the Cu-SiC-GNP powders milled for 2 h were fabricated. It was observed that the grains of as-received copper grew bigger and had a fine connection with each other with the increase of sintering temperatures. However, the ratio and size of pore and void were getting larger with the rising temperatures too. For the Cu-SiC-GNP composites, there was a similar trend in the morphology with the increase of temperatures. Nevertheless, the sintering temperatures turned out to be higher for a thorough sintering because of the high melting points of SiC and GNP.

As for the density, the density of sintered samples for Cu-SiC-GNP tended to increase from 700 to 750 ºC, but it decreased from 750 to 900 ºC. The density of pure copper showed a similar trend. Concerning the hardness, the hardness of Cu-SiC-GNP decreased from 750 to 900 ºC. The hardness decreased generally with the temperatures, but there was a little increase at 850 ºC because of the bigger effects of improvement in connection of grains. Overall the hardness of Cu-SiC-GNP decreased with the increase

of time from 700 to 900 ºC, ascribed to the rising void and porosity.

On the other hand, SEM was used to analyse the variation in morphology of powder samples of Cu, Cu-4 vol % SiC and Cu-4 vol % SiC-1 vol % GNP, with the increase of ball milling time. It was observed that these three materials shared a similar trend in morphology. Particles were flattened at first due to forces exerted from the milling balls. After 8 h ball milling, most particles turned into flakes with the same size, ascribed to the equilibrium between fracturing and cold welding.

XRD analysis was utilised to identify the chemical composition of the powder samples. There were only five peaks in powders milled from 2 to 8 h, meaning there was no undesirable reaction or a undetected volume of unexpected reaction existed after ball milling. At the same time, W-H method was to analyse the change of grain size with the prolonged ball milling time. The trends for different Cu, Cu-SiC and Cu-SiC-GNP were similar. First the grain size decreased to the minimum from 2 to 6 h and then increased again at 8 h, attributed to fracturing and cold welding. In addition, the grain size of Cu-SiC decreased continually from 8 to 20 h, ascribed to the equilibrium between fracturing and cold welding.

In the investigation of the morphology of sintered composites of Cu, Cu-SiC and Cu-SiC-GNP, the increasing ratio of flake particles corresponded to the distribution of powder morphology. A clearer phenomenon of flake particles stacking vertically was found as the ball milling time increased, which could be attributed to the compaction force of the mold set.

The density of Cu, Cu -SiC and Cu-SiC-GNP had different trends, but they tended to decrease with the ball milling time generally due to the work hardening and irregular shapes of particles. The densities of Cu-SiC and Cu-SiC-GNP were lower than that of Cu because of the addition of the low-density SiC and graphene. Furthermore, Cu, Cu

-SiC and Cu-SiC-GNP shared the same trend in hardness with the ball milling time in general. The hardness inclined to increase with the prolonged ball milling time, which could be explained by the work hardening and refinement of particles.

The compressive properties of Cu, Cu-SiC and Cu-SiC-GNP had different trends with the increase of ball milling time. There was enhancement in Cu and Cu-SiC with the increase of ball milling time. Nevertheless, the maximum of compressive stress of Cu-SiC-GNP had a tendency to decrease with the prolonged ball milling time, and the variation of compressive properties could be attributed to irregular morphology of Cu-SiC-GNP particles and the ball milling times that were not long enough to disperse both the SiC nanoparticles and graphene nanoplates homogeneously in the Cu matrix.

In this study, the advantage was that the theoretical density of Cu-SiC-GNP was smaller than that of Cu-SiC, and the compacting ability of Cu-SiC-GNP was better. Besides, the hardness of Cu-SiC-GNP was a little smaller than that of Cu-SiC, which could reduce the tool wear. Furthermore, the lubricant property of GNP could enhance the surface finish. It is expected that more advantages of Cu-SiC-GNP could be found in the further work.

6.2 Future work

As shown in the conclusion, the morphology of Cu-SiC powder milled for 20 h were flakes like Cu-SiC powders milled for 12 h. In addition, the grain size tended to decrease continually from 8 to 12 h. Therefore, Cu-SiC-GNP powders should be milled and fabricated from 8 to 20 h to see the further change in morphology and other relevant properties.

Since there is not obvious phenomenon to identify different chemical compositions by FSEM, complementary work (such as TEM) is advised to investigate the distribution and combination of GNP and SiC nanoparticles in the Cu matrix. At the same time,

etching might be a good choice to see the porosity distribution in the copper matrix. If the situation is not ideal, then methods like decorating SiC nanoparticles with GNP could be utilised to find out an appropriate route to make good use of GNP.

Tests of the electric conductivity will be conducted to investigate the superior properties of graphene in thermal and electrical conductivity. Based on the current research, tensile tests should be conducted to find the effect of GNP on the mechanical properties like ductility, since the graphene has a large surface area with two dimensional structures. As far as concerned of the tribological property, the wear measurements should be utilised to investigate the effect of GNP on the tribological behavior involving its fine lubrication. Furthermore, different percentages of SiC and GNP could be mixed to meet different requirements such as superior wear resistance and good electric conductivity.

References

[1] J. Zhu, L. Liu, H. Zhao, B. Shen, and W. Hu, "Microstructure and performance of electroformed Cu/nano-SiC composite," *Materials and Design,* Article vol. 28, no. 6, pp. 1958-1962, 2007.

[2] N. B. Dhokey and R. K. Paretkar, "Study of wear mechanisms in copper-based SiCp (20% by volume) reinforced composite," *Wear,* vol. 265, no. 1, pp. 117-133, 2008/06/25/ 2008.

[3] S. G. Sapate, A. Uttarwar, R. C. Rathod, and R. K. Paretkar, "Analyzing dry sliding wear behaviour of copper matrix composites reinforced with pre-coated SiCp particles," *Materials & Design,* vol. 30, no. 2, pp. 376-386, 2009/02/01/ 2009.

[4] P. Buchner, D. LÜTzenkirchen-Hecht, H.-H. Strehblow, and J. Uhlenbusch, "Production and characterization of nanosized Cu/O/SiC composite particles in a thermal r.f. plasma reactor," *Journal of Materials Science,* journal article vol. 34, no. 5, pp. 925-931, March 01 1999.

[5] J. Boselli, P. D. Pitcher, P. J. Gregson, and I. Sinclair, "Numerical modelling of particle distribution effects on fatigue in Al–SiCp composites," *Materials Science and Engineering: A,* vol. 300, no. 1, pp. 113-124, 2001/02/28/ 2001.

[6] V. V. Bhanuprasad, R. B. Bhat, A. K. Kuruvilla, K. S. Prasad, A. B. Pandey, and Y. R. Mahajan, "P/M processing of Al-SiC composites," *International journal of powder metallurgy,* vol. 27, no. 3, pp. 227-235, 1991.

[7] B. S. Ünlü, "Investigation of tribological and mechanical properties Al_2O_3–SiC reinforced Al composites manufactured by casting or P/M method," *Materials & Design,* vol. 29, no. 10, pp. 2002-2008, 12// 2008.

[8] H. Su, W. Gao, Z. Feng, and Z. Lu, "Processing, microstructure and tensile properties of nano-sized Al_2O_3 particle reinforced aluminum matrix composites," *Materials & Design,* vol. 36, no. 0, pp. 590-596, 4// 2012.

[9] M. Bastwros *et al.*, "Effect of ball milling on graphene reinforced Al6061 composite fabricated by semi-solid sintering," *Composites Part B: Engineering,* vol. 60, no. Supplement C, pp. 111-118, 2014/04/01/ 2014.

[10] I. El-Mahallawi, H. Abdelkader, L. Yousef, A. Amer, J. Mayer, and A. Schwedt, "Influence of Al_2O_3 nano-dispersions on microstructure features and mechanical properties of cast and T6 heat-treated Al Si hypoeutectic Alloys," *Materials Science and Engineering: A,* vol. 556, pp. 76-87, 2012.

[11] S. Tahamtan, A. Halvaee, M. Emamy, Z. Jiang, and A. F. Boostani, "Exploiting superior tensile properties of a novel network-structure AlA206 matrix composite by hybridizing micron-sized Al_3Ti with Al_2O_3 nano particulates," *Materials Science and Engineering: A,* vol. 619, pp. 190-198, 2014.

[12] S. Tahamtan, A. Halvaee, M. Emamy, and M. Zabihi, "Fabrication of Al/A206–Al_2O_3 nano/micro composite by combining ball milling and stir casting technology," *Materials & Design,* vol. 49, pp. 347-359, 2013.

[13] Y. Wu and G.-Y. Kim, "Carbon nanotube reinforced aluminum composite fabricated by semi-solid powder processing," *Journal of Materials Processing Technology,* vol. 211, no.

8, pp. 1341-1347, 2011.

[14] V. Dao, S. Zhao, W. Lin, and C. Zhang, "Effect of process parameters on microstructure and mechanical properties in AlSi9Mg connecting-rod fabricated by semi-solid squeeze casting," *Materials Science and Engineering: A,* vol. 558, pp. 95-102, 2012.

[15] I. El-Mahallawi *et al.*, "Influence of nanodispersions on strength–ductility properties of semisolid cast A356 Al alloy," *Materials Science and Technology,* vol. 26, no. 10, pp. 1226-1231, 2010.

[16] K. Hanada, Y. Murakoshi, H. Negishi, and T. Sano, "Microstructures and mechanical properties of Al-Li/SiCp composite produced by extrusion processing," *Journal of Materials Processing Technology,* vol. 63, no. 1, pp. 405-410, 1997/01/01/ 1997.

[17] M. J. Tan and X. Zhang, "Powder metal matrix composites: selection and processing," *Materials Science and Engineering: A,* vol. 244, no. 1, pp. 80-85, 1998/03/31/ 1998.

[18] Y. B. Liu, J. K. M. Kwok, S. C. Lim, L. Lu, and M. O. Lai, "Fabrication of Al-4.5Cu/15SiCp composites: I. Processing using mechanical alloying," *Journal of Materials Processing Technology,* vol. 37, no. 1, pp. 441-451, 1993/02/01/ 1993.

[19] L. Lu, M. O. Lai, and C. W. Ng, "Enhanced mechanical properties of an Al based metal matrix composite prepared using mechanical alloying," *Materials Science and Engineering: A,* vol. 252, no. 2, pp. 203-211, 1998/09/15/ 1998.

[20] R. Sankar and P. Singh, "Synthesis of 7075 Al/SiC particulate composite powders by mechanical alloying," *Materials Letters,* vol. 36, no. 1, pp. 201-205, 1998/07/01/ 1998.

[21] Z. ASLANOGLU, Y. KARAKAS, and M. L. ÖVECOGLU, "Switching performance of W-Ag electrical contacts fabricated by mechanical alloying," *International journal of powder metallurgy,* vol. 36, no. 8, pp. 35-43, 2000.

[22] J. B. Fogagnolo, E. M. Ruiz-Navas, M. H. Robert, and J. M. Torralba, "The effects of mechanical alloying on the compressibility of aluminium matrix composite powder," *Materials Science and Engineering: A,* vol. 355, no. 1, pp. 50-55, 2003/08/25/ 2003.

[23] N. Zhao, P. Nash, and X. Yang, "The effect of mechanical alloying on SiC distribution and the properties of 6061 aluminum composite," *Journal of Materials Processing Technology,* vol. 170, no. 3, pp. 586-592, 2005.

[24] Z. Razavi Hesabi, H. R. Hafizpour, and A. Simchi, "An investigation on the compressibility of aluminum/nano-alumina composite powder prepared by blending and mechanical milling," *Materials Science and Engineering: A,* vol. 454-455, no. Supplement C, pp. 89-98, 2007/04/25/ 2007.

[25] D. B. Miracle, "Metal matrix composites - From science to technological significance," *Composites Science and Technology,* Article vol. 65, no. 15-16 SPEC. ISS., pp. 2526-2540, 2005.

[26] J. W. Kaczmar, K. Pietrzak, and W. Włosiński, "The production and application of metal matrix composite materials," *Journal of Materials Processing Technology,* vol. 106, no. 1, pp. 58-67, 2000/10/31/ 2000.

[27] R. Q. Guo, P. K. Rohatgi, and D. Nath, "Preparation of aluminium-fly ash particulate composite by powder metallurgy technique," *Journal of Materials Science,* Article vol. 32, no. 15, pp. 3971-3974, 1997.

[28] S. Rawal, "Metal-matrix composites for space applications," *JOM,* Article vol. 53, no. 4, pp. 14-17, 2001.

[29] G. F. C. Efe, M. Ipek, S. Zeytin, and C. Bindal, "Fabrication and properties of sic reinforced copper-matrix-composite contact material," *Materiali in Tehnologije,* Article vol. 50, no. 4, pp. 585-590, 2016.

[30] J. R. Davis and A. S. M. I. H. Committee, *Copper and Copper Alloys*. ASM International, 2001.

[31] A. Nieto, A. Bisht, D. Lahiri, C. Zhang, and A. Agarwal, "Graphene reinforced metal and ceramic matrix composites: a review," *International Materials Reviews,* Review vol. 62, no. 5, pp. 241-302, 2017.

[32] Y. Cui, L. Wang, B. Li, G. Cao, and W. Fei, "Effect of ball milling on the defeat of few-layer graphene and properties of copper matrix composites," *Acta Metallurgica Sinica (English Letters),* Article vol. 27, no. 5, pp. 937-943, 2014.

[33] S. R. Allahkaram, S. Golroh, and M. Mohammadalipour, "Properties of Al_2O_3 nano-particle reinforced copper matrix composite coatings prepared by pulse and direct current electroplating," *Materials and Design,* Article vol. 32, no. 8-9, pp. 4478-4484, 2011.

[34] X. Niansuo and W. Jin, "Study on preparation of copper matrix composites reinforced by SiC and Graphite particles," in *2012 2nd International Conference on Consumer Electronics, Communications and Networks, CECNet 2012 - Proceedings*, 2012, pp. 1333-1336.

[35] S. C. Tjong, "Novel nanoparticle-reinforced metal matrix composites with enhanced mechanical properties," *Advanced Engineering Materials,* Review vol. 9, no. 8, pp. 639-652, 2007.

[36] P. H. C. Camargo, K. G. Satyanarayana, and F. Wypych, "Nanocomposites: Synthesis, structure, properties and new application opportunities," *Materials Research,* Review vol. 12, no. 1, pp. 1-39, 2009.

[37] Y. C. Kang and S. L. I. Chan, "Tensile properties of nanometric Al_2O_3 particulate-reinforced aluminum matrix composites," *Materials Chemistry and Physics,* Article vol. 85, no. 2-3, pp. 438-443, 2004.

[38] T. W. Clyne and P. J. Withers, *An Introduction to Metal Matrix Composites* (Cambridge Solid State Science Series). Cambridge: Cambridge University Press, 1993.

[39] E. Arzt, G. Dehm, P. Gumbsch, O. Kraft, and D. Weiss, "Interface controlled plasticity in metals: Dispersion hardening and thin film deformation," *Progress in Materials Science,* Article vol. 46, no. 3-4, pp. 283-307, 2001.

[40] M. Dao, L. Lu, R. J. Asaro, J. T. M. De Hosson, and E. Ma, "Toward a quantitative understanding of mechanical behavior of nanocrystalline metals," *Acta Materialia,* Article vol. 55, no. 12, pp. 4041-4065, 2007.

[41] K. U. Kainer, *Metal Matrix Composites: Custom-made Materials for Automotive and Aerospace Engineering* (Metal Matrix Composites: Custom-made Materials for Automotive and Aerospace Engineering). 2006, pp. 1-314.

[42] Y. Sahin and M. Acilar, "Production and properties of SiCp-reinforced aluminium alloy composites," *Composites Part A: Applied Science and Manufacturing,* Article vol. 34, no. 8, pp. 709-718, 2003.

[43] F. Chi, M. Schmerling, Z. Eliezer, H. L. Marcus, and M. E. Fine, "Preparation of Cu-TiN alloy by external nitridation in combination with mechanical alloying," *Materials Science and Engineering: A,* vol. 190, no. 1, pp. 181-186, 1995/01/01/ 1995.

[44] J. B. Correia, H. A. Davies, and C. M. Sellars, "Strengthening in rapidly solidified age hardened Cu-Cr and Cu-Cr-Zr alloys," *Acta Materialia,* vol. 45, no. 1, pp. 177-190, 1997/01/01/ 1997.

[45] S. C. Tjong and K. C. Lau, "Tribological behaviour of SiC particle-reinforced copper matrix composites," *Materials Letters,* Article vol. 43, no. 5, pp. 274-280, 2000.

[46] Y. Zhan, G. Zhang, and Y. Zhuang, "Wear transitions in particulate reinforced copper matrix composites," *Materials Transactions,* Conference Paper vol. 45, no. 7, pp. 2332-2338, 2004.

[47] M. R. Akbarpour and S. Alipour, "Wear and friction properties of spark plasma sintered SiC/Cu nanocomposites," *Ceramics International,* Article vol. 43, no. 16, pp. 13364-13370, 2017.

[48] K. Song, X. Guo, S. Liang, P. Zhao, and Y. Zhang, "Relationship between interfacial stress and thermal expansion coefficient of copper-matrix composites with different reinforced phases," *Materials Science and Technology (United Kingdom),* Article vol. 30, no. 2, pp. 171-175, 2014.

[49] F. Shehata, "Preparation and properties of Al_2O_3 nanoparticle reinforced copper matrix composites by in situ processing," *Materials in engineering,* vol. 30, no. 7, pp. 2756-2762, 2009.

[50] T. Schubert *et al.*, "Interfacial design of Cu/SiC composites prepared by powder metallurgy for heat sink applications," *Composites Part A: Applied Science and Manufacturing,* Article vol. 38, no. 12, pp. 2398-2403, 2007.

[51] W. Zein Eddine, P. Matteazzi, and J. P. Celis, "Mechanical and tribological behavior of nanostructured copper-alumina cermets obtained by Pulsed Electric Current Sintering," *Wear,* Article vol. 297, no. 1-2, pp. 762-773, 2013.

[52] G. Celebi Efe, T. Yener, I. Altinsoy, M. Ipek, S. Zeytin, and C. Bindal, "The effect of sintering temperature on some properties of Cu–SiC composite," *Journal of Alloys and Compounds,* vol. 509, no. 20, pp. 6036-6042, 2011/05/19/ 2011.

[53] M. Rahimian, N. Ehsani, N. Parvin, and H. r. Baharvandi, "The effect of particle size, sintering temperature and sintering time on the properties of Al–Al_2O_3 composites, made by powder metallurgy," *Journal of Materials Processing Technology,* vol. 209, no. 14, pp. 5387-5393, 2009/07/19/ 2009.

[54] R. M. German, "Powder metallurgy of iron and steel," *John! Wiley & Sons, Inc, 605 Third Ave, New York, NY 10016, USA, 1998. 496,* 1998.

[55] M. Cabeza *et al.*, "Effect of high energy ball milling on the morphology, microstructure and properties of nano-sized TiC particle-reinforced 6005A aluminium alloy matrix composite," *Powder Technology,* vol. 321, pp. 31-43, 2017/11/01/ 2017.

[56] J. B. Fogagnolo, F. Velasco, M. H. Robert, and J. M. Torralba, "Effect of mechanical alloying on the morphology, microstructure and properties of aluminium matrix composite powders," *Materials Science and Engineering: A,* vol. 342, no. 1, pp. 131-143, 2003/02/15/ 2003.

[57] K. Gan and M. Gu, "The compressibility of Cu/SiCp powder prepared by high-energy ball milling," *Journal of Materials Processing Technology,* vol. 199, no. 1, pp. 173-177, 2008/04/01/ 2008.

[58] R. Panelli and F. Ambrozio Filho, "Compaction equation and its use to describe powder

consolidation behavior," *Powder metallurgy,* vol. 41, no. 2, pp. 131-133, 1998.

[59] M. R. Akbarpour, E. Salahi, F. Alikhani Hesari, H. S. Kim, and A. Simchi, "Effect of nanoparticle content on the microstructural and mechanical properties of nano-SiC dispersed bulk ultrafine-grained Cu matrix composites," *Materials and Design,* Article vol. 52, pp. 881-887, 2013.

[60] A. Fathy, F. Shehata, M. Abdelhameed, and M. Elmahdy, "Compressive and wear resistance of nanometric alumina reinforced copper matrix composites," *Materials & Design (1980-2015),* vol. 36, pp. 100-107, 2012.

[61] B. T. Al-Mosawi, D. Wexler, and A. Calka, "Characterization and mechanical properties of α- Al_2O_3 particle reinforced aluminium matrix composites, synthesized via uniball magneto-milling and uniaxial hot pressing," *Advanced Powder Technology,* vol. 28, no. 3, pp. 1054-1064, 2017/03/01/ 2017.

[62] F. Safari, R. Azari Khosroshahi, and A. Zolriasatein, "Wear behavior of copper matrix composites reinforced by γ-Cu_5Zn_8 nanoparticles," *Powder Technology,* Article vol. 318, pp. 549-557, 2017.

[63] M. R. Akbarpour, E. Salahi, F. A. Hesari, E. Y. Yoon, H. S. Kim, and A. Simchi, "Microstructural development and mechanical properties of nanostructured copper reinforced with SiC nanoparticles," *Materials Science and Engineering A,* Article vol. 568, pp. 33-39, 2013.

[64] T. S. M. El-Sayed Youssef El-Kady, Ali Abdel-Aziz Ali, " On the electrical and thermal conductivities of cast A356/Al2O3 metal matrix nanocomposites," *Materials Science and Applicatins,* pp. 1180-1187, 2011, 2 2011.

[65] K. Chu *et al.*, "Fabrication and effective thermal conductivity of multi-walled carbon nanotubes reinforced Cu matrix composites for heat sink applications," *Composites Science and Technology,* vol. 70, no. 2, pp. 298-304, 2010/02/01/ 2010.

[66] K. S. Novoselov *et al.*, "Electric field in atomically thin carbon films," *Science,* Article vol. 306, no. 5696, pp. 666-669, 2004.

[67] S. Stankovich *et al.*, "Synthesis of graphene-based nanosheets via chemical reduction of exfoliated graphite oxide," *Carbon,* vol. 45, no. 7, pp. 1558-1565, 2007/06/01/ 2007.

[68] S. F. Bartolucci *et al.*, "Graphene–aluminum nanocomposites," *Materials Science and Engineering: A,* vol. 528, no. 27, pp. 7933-7937, 2011/10/15/ 2011.

[69] J. Wang, Z. Li, G. Fan, H. Pan, Z. Chen, and D. Zhang, "Reinforcement with graphene nanosheets in aluminum matrix composites," *Scripta Materialia,* vol. 66, no. 8, pp. 594-597, 2012/04/01/ 2012.

[70] L.-Y. Chen *et al.*, "Novel nanoprocessing route for bulk graphene nanoplatelets reinforced metal matrix nanocomposites," *Scripta Materialia,* vol. 67, no. 1, pp. 29-32, 2012/07/01/ 2012.

[71] K. Chu and C. Jia, "Enhanced strength in bulk graphene-copper composites," *Physica Status Solidi (A) Applications and Materials Science,* Article vol. 211, no. 1, pp. 184-190, 2014.

[72] W. J. Kim, T. J. Lee, and S. H. Han, "Multi-layer graphene/copper composites: Preparation using high-ratio differential speed rolling, microstructure and mechanical properties," *Carbon,* Article vol. 69, pp. 55-65, 2014.

[73] M. Li, H. Che, X. Liu, S. Liang, and H. Xie, "Highly enhanced mechanical properties in Cu matrix composites reinforced with graphene decorated metallic nanoparticles," *Journal of*

Materials Science, Article vol. 49, no. 10, pp. 3725-3731, 2014.

[74] H. Yue *et al.*, "Effect of ball-milling and graphene contents on the mechanical properties and fracture mechanisms of graphene nanosheets reinforced copper matrix composites," *Journal of Alloys and Compounds,* Article vol. 691, pp. 755-762, 2017.

[75] Y. Tang, X. Yang, R. Wang, and M. Li, "Enhancement of the mechanical properties of graphene-copper composites with graphene-nickel hybrids," *Materials Science and Engineering A,* Article vol. 599, pp. 247-254, 2014.

[76] J. Hwang *et al.*, "Enhanced mechanical properties of graphene/copper nanocomposites using a molecular-level mixing process," *Advanced Materials,* Article vol. 25, no. 46, pp. 6724-6729, 2013.

[77] K. Jagannadham, "Orientation dependence of thermal conductivity in copper-graphene composites," *Journal of Applied Physics,* Article vol. 110, no. 7, 2011, Art. no. 074901.

[78] K. Jagannadham, "Volume fraction of graphene platelets in copper-graphene composites," *Metallurgical and Materials Transactions A: Physical Metallurgy and Materials Science,* Article vol. 44, no. 1, pp. 552-559, 2013.

[79] K. Zhang, "Fabrication of copper nanoparticles/graphene oxide composites for surface-enhanced Raman scattering," *Applied Surface Science,* Article vol. 258, no. 19, pp. 7327-7329, 2012.

[80] G. Renguo, L. Chao, Z. Zhanyong, C. Runze, and L. Chunming, "Study on preparation of graphene and Al-graphene Composite," *Rare Metal Materials and Engineering S,* vol. 2, 2012.

[81] M. Bastwros, G.-Y. Kim, K. Zhang, and S. Wang, "Fabrication of graphene reinforced aluminum composite by semi-solid processing," in *ASME 2013 International Mechanical Engineering Congress and Exposition*, 2013, pp. V02BT02A030-V02BT02A030: American Society of Mechanical Engineers.

[82] Z. Li *et al.*, "Uniform dispersion of graphene oxide in aluminum powder by direct electrostatic adsorption for fabrication of graphene/aluminum composites," *Nanotechnology,* vol. 25, no. 32, p. 325601, 2014.

[83] C. YANG, "Research of graphene-reinforced aluminum matrix nanocomposites," *Journal of Materials Engineering,* vol. 1, no. 4, pp. 1-6, 2011.

[84] J. Li *et al.*, "Microstructure and tensile properties of bulk nanostructured aluminum/graphene composites prepared via cryomilling," *Materials Science and Engineering: A,* vol. 626, pp. 400-405, 2015.

[85] T. S. Koltsova *et al.*, "New hybrid copper composite materials based on carbon nanostructures," *Journal of Materials Science and Engineering B,* vol. 2, no. 4, pp. 240-246, 2012.

[86] Y. Kim *et al.*, "Strengthening effect of single-atomic-layer graphene in metal–graphene nanolayered composites," *Nature communications,* vol. 4, p. ncomms3114, 2013.

[87] C. L. Pavithra, B. V. Sarada, K. V. Rajulapati, T. N. Rao, and G. Sundararajan, "A new electrochemical approach for the synthesis of copper-graphene nanocomposite foils with high hardness," *Scientific reports,* vol. 4, p. 4049, 2014.

[88] G. Xie, M. Forslund, and J. Pan, "Direct electrochemical synthesis of reduced graphene oxide (rGO)/copper composite films and their electrical/electroactive properties," *ACS applied materials & interfaces,* vol. 6, no. 10, pp. 7444-7455, 2014.

[89] C. Zhao and J. Wang, "Fabrication and tensile properties of graphene/copper composites prepared by electroless plating for structrual applications," *physica status solidi (a),* vol. 211, no. 12, pp. 2878-2885, 2014.

[90] J. Dutkiewicz *et al.*, "Microstructure and properties of bulk copper matrix composites strengthened with various kinds of graphene nanoplatelets," *Materials Science and Engineering A,* Article vol. 628, pp. 124-134, 2015.

[91] K. Jagannadham, "Electrical conductivity of copper–graphene composite films synthesized by electrochemical deposition with exfoliated graphene platelets," *Journal of Vacuum Science & Technology B, Nanotechnology and Microelectronics: Materials, Processing, Measurement, and Phenomena,* vol. 30, no. 3, p. 03D109, 2012.

[92] S. F. Hassan and M. Gupta, "Effect of different types of nano-size oxide participates on microstructural and mechanical properties of elemental Mg," *Journal of Materials Science,* Article vol. 41, no. 8, pp. 2229-2236, 2006.

[93] M. Habibnejad-Korayem, R. Mahmudi, and W. J. Poole, "Enhanced properties of Mg-based nano-composites reinforced with Al_2O_3 nano-particles," *Materials Science and Engineering A,* Article vol. 519, no. 1-2, pp. 198-203, 2009.

[94] S.-M. Paek, E. Yoo, and I. Honma, "Enhanced Cyclic Performance and Lithium Storage Capacity of SnO_2/Graphene Nanoporous Electrodes with Three-Dimensionally Delaminated Flexible Structure," *Nano Letters,* vol. 9, no. 1, pp. 72-75, 2009/01/14 2009.

[95] L. S. Zhang *et al.*, "Mono dispersed SnO_2 nanoparticles on both sides of single layer graphene sheets as anode materials in Li-ion batteries," *Journal of Materials Chemistry,* Article vol. 20, no. 26, pp. 5462-5467, 2010.

[96] V. Singh, D. Joung, L. Zhai, S. Das, S. I. Khondaker, and S. Seal, "Graphene based materials: Past, present and future," *Progress in Materials Science,* vol. 56, no. 8, pp. 1178-1271, 2011/10/01/ 2011.

[97] I. V. Lightcap, T. H. Kosel, and P. V. Kamat, "Anchoring semiconductor and metal nanoparticles on a two-dimensional catalyst mat. storing and shuttling electrons with reduced graphene oxide," *Nano Letters,* Article vol. 10, no. 2, pp. 577-583, 2010.

[98] A. F. Boostani *et al.*, "Graphene sheets encapsulating SiC nanoparticles: A roadmap towards enhancing tensile ductility of metal matrix composites," *Materials Science and Engineering: A,* vol. 648, no. Supplement C, pp. 92-103, 2015/11/11/ 2015.

[99] A. Fadavi Boostani *et al.*, "Enhanced tensile properties of aluminium matrix composites reinforced with graphene encapsulated SiC nanoparticles," *Composites Part A: Applied Science and Manufacturing,* vol. 68, no. Supplement C, pp. 155-163, 2015/01/01/ 2015.

[100] A. Fadavi Boostani *et al.*, "Graphene tweaking Hamaker constant of SiC nanoparticles: A new horizon to solve the conflict between strengthening and toughening," *Scripta Materialia,* vol. 118, no. Supplement C, pp. 65-69, 2016/06/01/ 2016.

[101] A. Fadavi Boostani *et al.*, "Solvothermal-assisted graphene encapsulation of SiC nanoparticles: A new horizon toward toughening aluminium matrix nanocomposites," *Materials Science and Engineering: A,* vol. 653, no. Supplement C, pp. 99-107, 2016/01/20/ 2016.

[102] A. Fadavi Boostani *et al.*, "Strengthening mechanisms of graphene sheets in aluminium matrix nanocomposites," *Materials & Design,* vol. 88, no. Supplement C, pp. 983-989, 2015/12/25/ 2015.

[103] J. W. Kaczmar, K. Pietrzak, and W. Wlosiński, "Production and application of metal matrix composite materials," *Journal of Materials Processing Technology,* Article vol. 106, no. 1-3, pp. 58-67, 2000.

[104] R. Casati and M. Vedani, "Metal Matrix Composites Reinforced by Nano-Particles—A Review," *Metals,* vol. 4, no. 1, 2014.

[105] H. K. Kang and S. B. Kang, "Thermal decomposition of silicon carbide in a plasma-sprayed Cu/SiC composite deposit," *Materials Science and Engineering A,* Article vol. 428, no. 1-2, pp. 336-345, 2006.

[106] J. Lan, Y. Yang, and X. Li, "Microstructure and microhardness of SiC nanoparticles reinforced magnesium composites fabricated by ultrasonic method," *Materials Science and Engineering A,* Article vol. 386, no. 1-2, pp. 284-290, 2004.

[107] J. Zhu, L. Liu, G. Hu, B. Shen, W. Hu, and W. Ding, "Study on composite electroforming of Cu/SiCp composites," *Materials Letters,* Article vol. 58, no. 10, pp. 1634-1637, 2004.

[108] L. Kollo, M. Leparoux, C. R. Bradbury, C. Jäggi, E. Carreño-Morelli, and M. Rodríguez-Arbaizar, "Investigation of planetary milling for nano-silicon carbide reinforced aluminium metal matrix composites," *Journal of Alloys and Compounds,* vol. 489, no. 2, pp. 394-400, 2010/01/21/ 2010.

[109] M. Tavoosi, F. Karimzadeh, and M. H. Enayati, "Fabrication of Al–Zn/α-Al_2O_3 nanocomposite by mechanical alloying," *Materials Letters,* vol. 62, no. 2, pp. 282-285, 2008/01/31/ 2008.

[110] M. Barmouz, P. Asadi, M. K. Besharati Givi, and M. Taherishargh, "Investigation of mechanical properties of Cu/SiC composite fabricated by FSP: Effect of SiC particles' size and volume fraction," *Materials Science and Engineering A,* Article vol. 528, no. 3, pp. 1740-1749, 2011.

[111] G. Celebi Efe, M. Ipek, S. Zeytin, and C. Bindal, "An investigation of the effect of SiC particle size on Cu-SiC composites," *Composites Part B: Engineering,* Article vol. 43, no. 4, pp. 1813-1822, 2012.

[112] O. Güler and E. Evin, "The investigation of contact performance of oxide reinforced copper composite via mechanical alloying," *Journal of Materials Processing Technology,* Article vol. 209, no. 3, pp. 1286-1290, 2009.

[113] K. B. Nie, X. J. Wang, L. Xu, K. Wu, X. S. Hu, and M. Y. Zheng, "Influence of extrusion temperature and process parameter on microstructures and tensile properties of a particulate reinforced magnesium matrix nanocomposite," *Materials & Design (1980-2015),* vol. 36, no. Supplement C, pp. 199-205, 2012/04/01/ 2012.

[114] D. Gu, Y.-C. Hagedorn, W. Meiners, K. Wissenbach, and R. Poprawe, "Nanocrystalline TiC reinforced Ti matrix bulk-form nanocomposites by Selective Laser Melting (SLM): Densification, growth mechanism and wear behavior," *Composites Science and Technology,* vol. 71, no. 13, pp. 1612-1620, 2011/09/09/ 2011.

[115] V. C. Nardone and K. M. Prewo, "On the strength of discontinuous silicon carbide reinforced aluminum composites," *Scripta Metallurgica,* vol. 20, no. 1, pp. 43-48, 1986/01/01/ 1986.

[116] Z. Zhang and D. L. Chen, "Contribution of Orowan strengthening effect in particulate-reinforced metal matrix nanocomposites," *Materials Science and Engineering: A,* vol. 483-484, no. Supplement C, pp. 148-152, 2008/06/15/ 2008.

[117] Z. Zhang and D. L. Chen, "Consideration of Orowan strengthening effect in particulate-reinforced metal matrix nanocomposites: A model for predicting their yield strength," *Scripta Materialia,* vol. 54, no. 7, pp. 1321-1326, 2006/04/01/ 2006.

[118] A. Sanaty-Zadeh, "Comparison between current models for the strength of particulate-reinforced metal matrix nanocomposites with emphasis on consideration of Hall–Petch effect," *Materials Science and Engineering: A,* vol. 531, no. Supplement C, pp. 112-118, 2012/01/01/ 2012.

[119] D. Hull and D. J. Bacon, *Introduction to dislocations*. Butterworth-Heinemann, 2001.

[120] R. E. Smallman and A. Ngan, *Physical metallurgy and advanced materials*. Butterworth-Heinemann, 2011.

[121] D. Hull and T. Clyne, *An introduction to composite materials*. Cambridge university press, 1996.

[122] C. Suryanarayana, "Mechanical alloying and milling," *Progress in Materials Science,* vol. 46, no. 1, pp. 1-184, 2001/01/01/ 2001.

[123] P. Scardi, M. Leoni, and R. Delhez, "Line broadening analysis using integral breadth methods: a critical review," *Journal of Applied Crystallography,* vol. 37, no. 3, pp. 381-390, 2004.

[124] H. Kuhn and D. Medlin, "ASM Handbook. Volume 8: Mechanical Testing and Evaluation," *ASM International, Member/Customer Service Center, Materials Park, OH 44073-0002, USA, 2000. 998,* 2000.

[125] P. Katiyar, "Processing, microstructural and mechanical characterization of mechanically alloyed Al-Al2O3 nanocomposites," 2004.

[126] T. W. Gustafson, P. C. Panda, G. Song, and R. Raj, "Influence of microstructural scale on plastic flow behavior of metal matrix composites," *Acta Materialia,* vol. 45, no. 4, pp. 1633-1643, 1997/04/01/ 1997.

[127] J. Bartolomé, G. Bruno, and A. DeAza, "Neutron diffraction residual stress analysis of zirconia toughened alumina (ZTA) composites," *Journal of the European Ceramic Society,* vol. 28, no. 9, pp. 1809-1814, 2008.

[128] M. R. Akbarpour, E. Salahi, F. Alikhani Hesari, A. Simchi, and H. S. Kim, "Microstructure and compressibility of SiC nanoparticles reinforced Cu nanocomposite powders processed by high energy mechanical milling," *Ceramics International,* Article vol. 40, no. 1 PART A, pp. 951-960, 2014.

[129] B. Prabhu, C. Suryanarayana, L. An, and R. Vaidyanathan, "Synthesis and characterization of high volume fraction Al–Al_2O_3 nanocomposite powders by high-energy milling," *Materials Science and Engineering: A,* vol. 425, no. 1, pp. 192-200, 2006/06/15/ 2006.

[130] C. Suryanarayana, "Does a disordered γ-TiAl phase exist in mechanically alloyed TiAl powders?," *Intermetallics,* vol. 3, no. 2, pp. 153-160, 1995/01/01/ 1995.

[131] N. Abu-Warda, M. V. Utrilla, M. D. Escalera, E. Otero, and M. D. López, "The effect of TiB2 content on the properties of AA6005/TiB2 nanocomposites fabricated by mechanical alloying method," *Powder Technology,* vol. 328, pp. 235-244, 2018/04/01/ 2018.

[132] A. Wagih and A. Fathy, "Experimental investigation and FE simulation of nano-indentation on Al–Al_2O_3 nanocomposites," *Advanced Powder Technology,* vol. 27, no. 2, pp. 403-410, 2016/03/01/ 2016.

[133] A. Wagih and A. Fathy, "Experimental investigation and FE simulation of spherical

indentation on nano-alumina reinforced copper-matrix composite produced by three different techniques," *Advanced Powder Technology,* vol. 28, no. 8, pp. 1954-1965, 2017/08/01/ 2017.

[134] C.-L. Chen and C.-H. Lin, "Effect of Y_2O_3 and TiC Reinforcement Particles on Intermetallic Formation and Hardness of Al6061 Composites via Mechanical Alloying and Sintering," *Metallurgical and Materials Transactions A,* journal article vol. 46, no. 8, pp. 3687-3695, August 01 2015.